Supplementary Information

Emergence of Lignin-Carbohydrate Interactions During Plant Stem Maturation Visualized by Solid-State NMR

Peng Xiao[1,#], Sarah A. Pfaff[2,#], Wancheng Zhao[1†], Debkumar Debnath[1], Cameron S. Vojvodin[1], Chang-Jun Liu[3], Daniel J. Cosgrove[2*], Tuo Wang[1*]

[1] Department of Chemistry, Michigan State University, East Lansing, MI 48824, USA

[2] Department of Biology, Pennsylvania State University, University Park, PA 16802, USA

[3] Biology Department, Brookhaven National Laboratory, Upton, NY 11973, USA

[#] These authors contributed equally

[†] Present address: Laboratory of Chemical Physics, National Institute of Diabetes and Digestive and Kidney Diseases, National Institutes of Health, Bethesda, MD 20892, USA

[*]Corresponding author: dcosgrove@psu.edu; wangtuo1@msu.edu

This file includes:

Supplementary Figures 1-24, Supplementary Tables 1-6, and Supplementary References

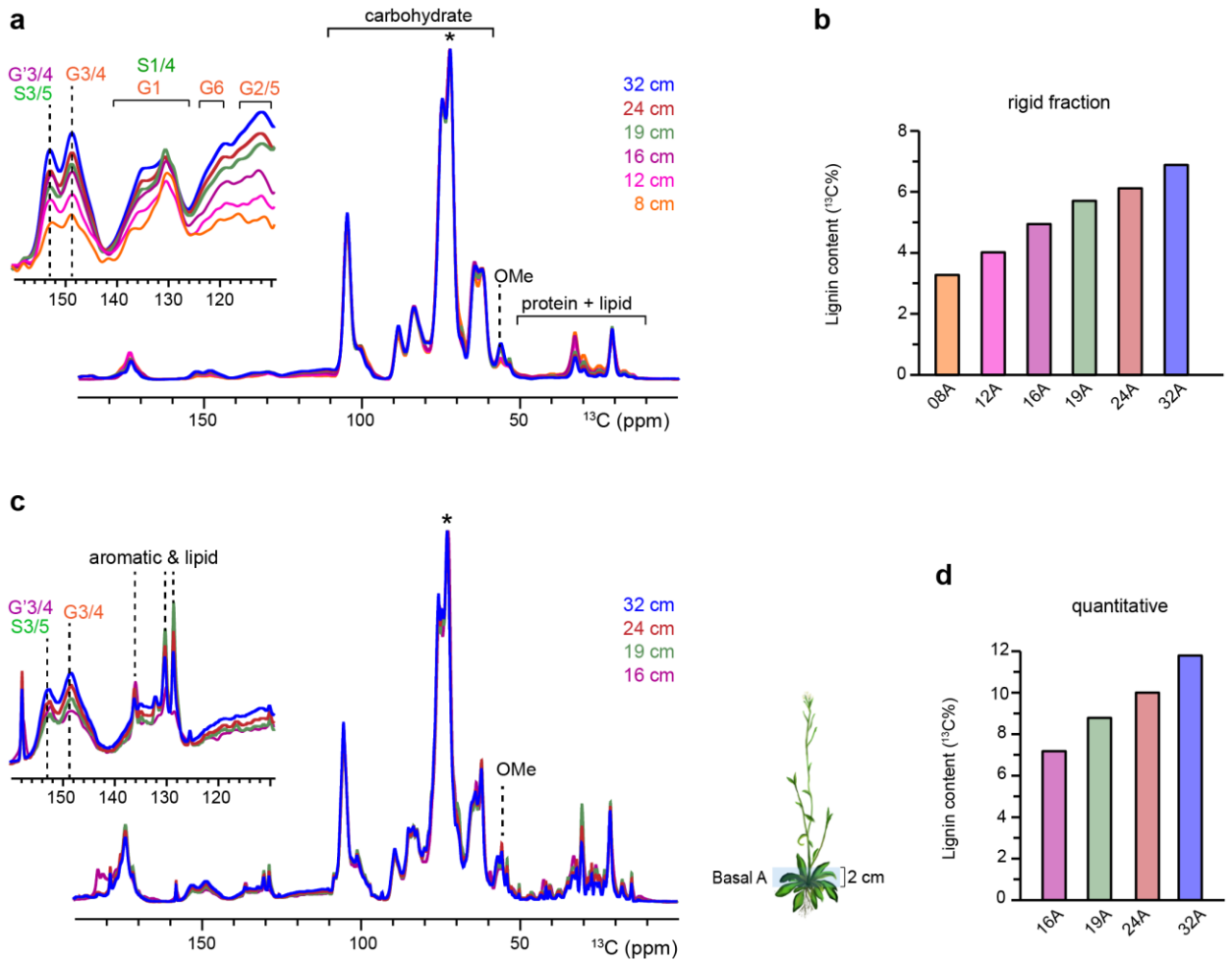

Supplementary Figure 1. Lignification of WT *Arabidopsis* stems at various growth stages. (**a**) 1D CP spectra showing rigid components of the WT *Arabidopsis* samples. All spectra are normalized with respect to the highest carbohydrate peak (asterisk). Zoomed-in view was provided for the lignin aromatic region showing the changes in the lignin content. The samples include the basal A of the stem grew to heights of 8, 12, 16, 19, 24 and 32 cm. (**b**) Overall lignin content in the rigid fraction of whole cell estimated from the 1D CP spectra of each sample. (**c**) 1D ^{13}C DP spectra with long recycle delays of 35 s showing quantitative ^{13}C composition of the WT *Arabidopsis* samples. The samples include the basal A of the stem grown to heights of 16, 19, 24 and 32 cm. The illustrations on the right show the inflorescence segment (basal A, 0-2 cm) used for all experiments. All spectra are normalized with respect to the highest carbohydrate peak (asterisk). Zoomed-in view region includes signals from the lignin aromatic carbons, fatty acyl chain carbons in lipids, as well as sidechain carbons in aromatic amino acid residues. The aromatic residues and lipids here are more dynamic and their signals manifest as strong sharp peaks at around 136, 132, 130 and 128 ppm. The unambiguous lignin peaks are at around 152.5 ppm (S3/5, G'3/4) and 148.5 ppm (G3/4); their peak shapes and positions are largely invariant compared to their counterparts in the CP spectra. (**d**) Quantitative analysis of overall lignin content in whole cell from ^{13}C DP spectra of each sample. Source data are provided as a Source Data file.

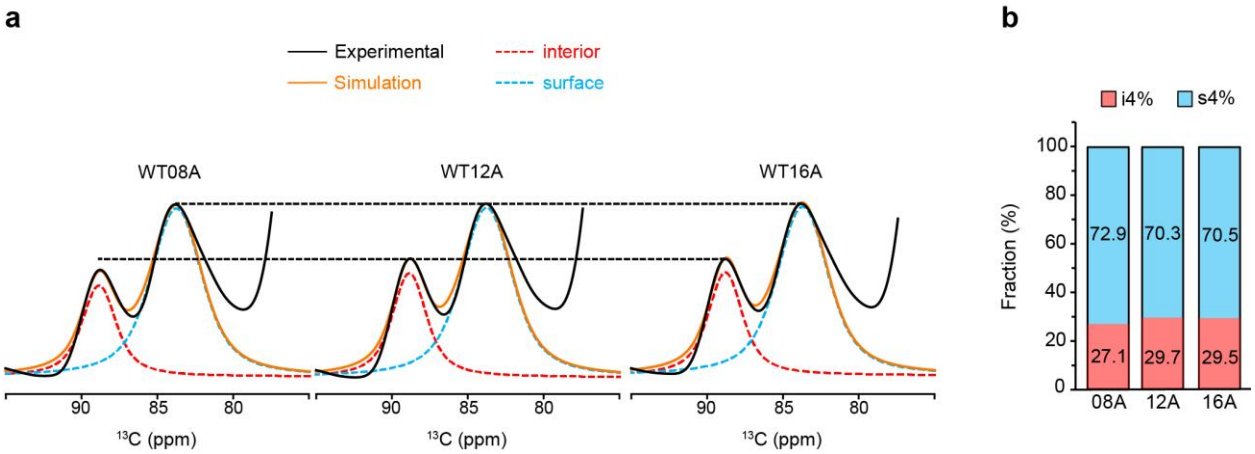

Supplementary Figure 2. Estimation of surface and interior chains of cellulose in wild-type stems. (**a**) Spectral deconvolution of the unambiguous cellulose region in 1D CP spectra for samples WT-08/12/16A. The resolved peaks for interior and surface cellulose are i4 (89 ppm) and s4 (84 ppm), respectively, and all spectra were normalized to the s4 peak. The experimentally measured spectra (black) are overlaid with the simulated spectra (orange) reconstructed from the deconvoluted peaks. The deconvolution was performed with ssNake software[1], using Lorentzian/Gaussian model. (**b**) Fractions of interior and surface cellulose chains in each sample. The percentages were estimated from the integrals of each deconvoluted peak of i4 and s4 and were indicated on each bar. Source data are provided as a Source Data file.

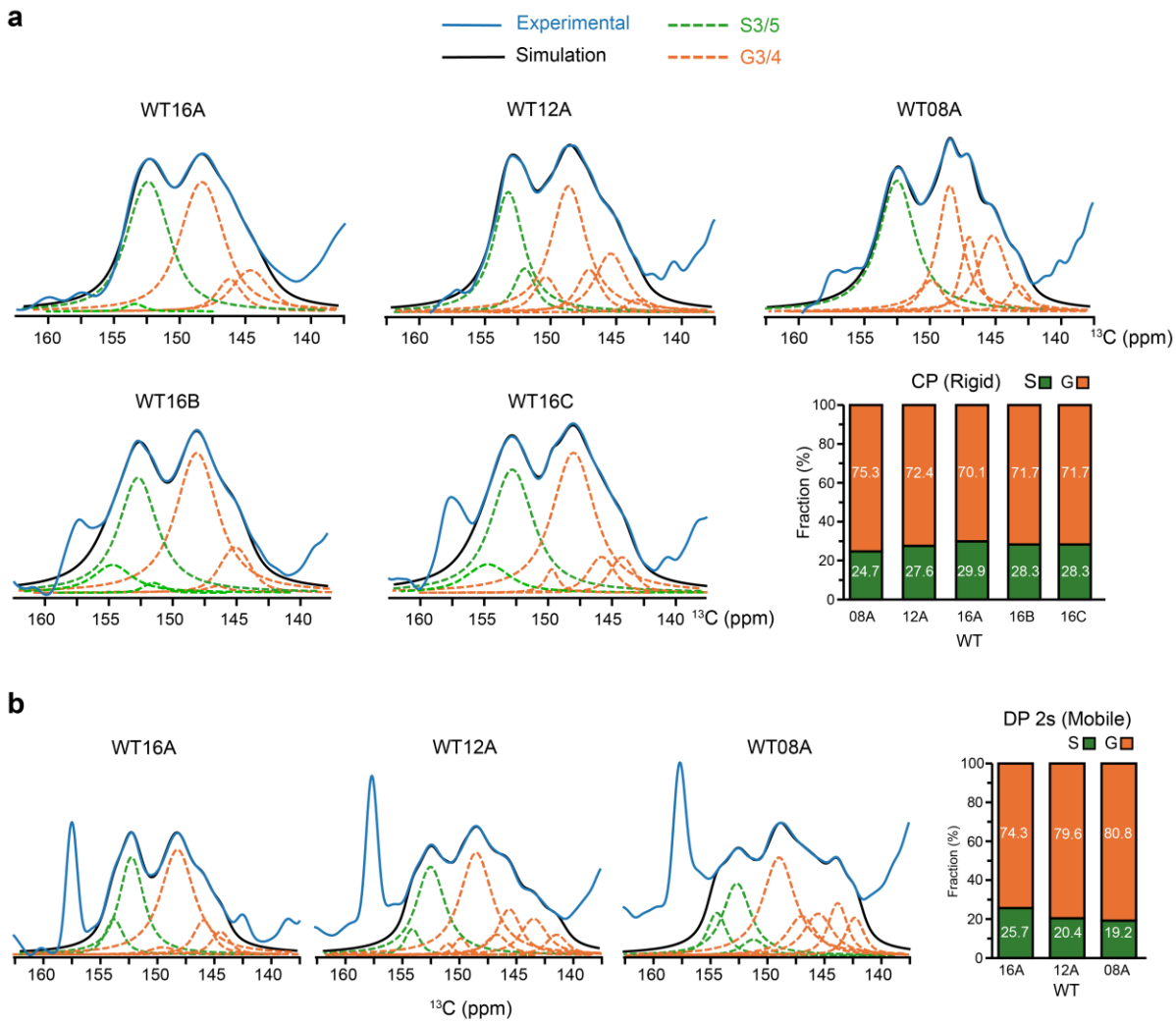

Supplementary Figure 3. Estimation of S and G content in wild-type stems. (**a**) Spectral deconvolution of the signature lignin region for (**a**) 1D CP spectra of samples WT-08A/12A/16A/16B/16C, and (**b**) 1D DP 2s spectra of samples WT-08A/12A/16A. The experimentally measured spectra (blue) are overlaid with the simulated spectra (black) reconstructed from the deconvoluted peaks. The fractions of the S and G units in each sample are shown on the right, with the percentages indicated on each bar. Estimations were based on the integrals of deconvoluted peaks of each unit, factored in the contribution factors outlined in **Supplementary Table 5**. All deconvolutions were performed with ssNake software, using Lorentzian/Gaussian model. Source data are provided as a Source Data file.

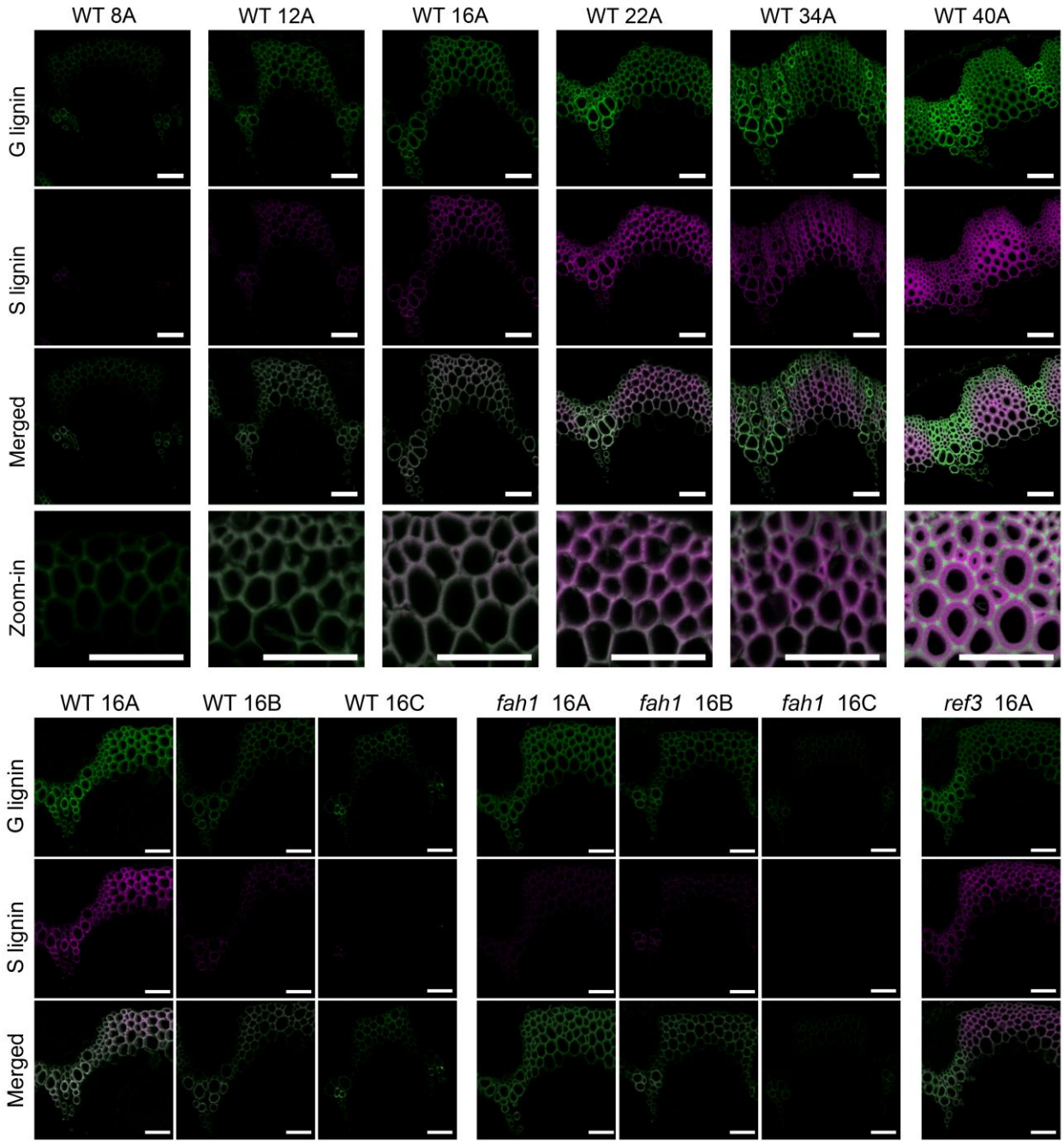

Supplementary Figure 4. Single channel and overlay images of representative Mäule-stained *Arabidopsis* stem cross sections. Fluorescence images depict the distribution of G-lignin (green) and S-lignin (purple) in the lignified tissues of basal segments of inflorescences across a developmental gradient in wild-type (top four rows); zoomed-in views for the wild-type are shown as the fourth row. The comparison with two mutants is displayed as the bottom three rows. Scale bars = 50 μm. Representative images from three biological replicates, with consistent results across two independent staining sessions.

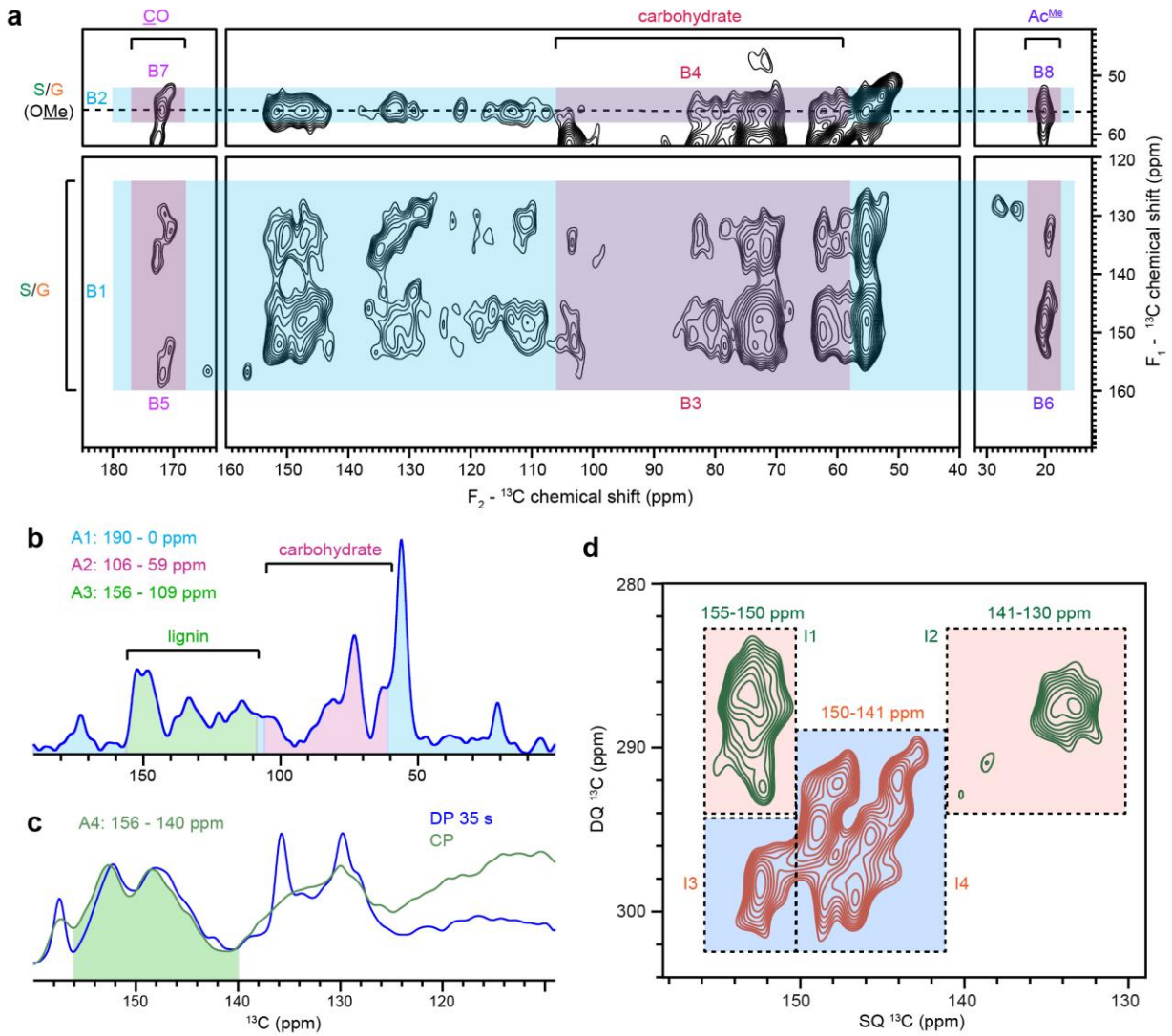

Supplementary Figure 5. Integration areas used for analyzing lignin content and interactions. (**a**) Integration areas (B1-B8) used for the analysis of 2D dipolar-gated PDSD spectra (1 s mixing time, long-range). Areas highlighted in blue indicate all ^{13}C signals originated from lignin ring carbons and OMe carbons. The OMe carbons are mainly from the lignin methyl ether (56 ppm, indicated by horizontal dashed line) and may include minor pectin methyl ester contribution (53 ppm). Areas highlighted in dark magenta indicate cross-peaks between lignin aromatic carbons and carbohydrate carbons. (**b**) 1D cross section extracted from the 2D spectrum. Area A1 represents all ^{13}C signals in the system. A2 includes carbohydrate signals. A3 includes lignin aromatic carbon sites aside from S2/6. The signals in A3 region are primarily from lignin in the CP experiment but also contain contributions from proteins and lipids in the DP experiment. (**c**) Zoomed-in view of the aromatic region with both the CP spectrum (green) and DP spectrum (blue). A4 indicates the unique lignin peak region used for the quantitative lignin content analysis. The line shape of this region is invariant between the CP and DP spectrum. (**d**) Unique S and G peak regions in 2D J-INADEQUATE spectrum. The integration regions I1-I4 were used for estimating the S/G ratio and I1&I3 were used for estimating the contribution factor of S and G units in the overlapping region of 1D spectra (A4). I1 and I2 include S3/5 and S4 peaks, respectively; I3 and I4 include all G3/4 peaks. The I1/I3 ratio is 1.7 in the WT sample. The chemical shift ranges for each area are summarized in **Supplementary Table 5**.

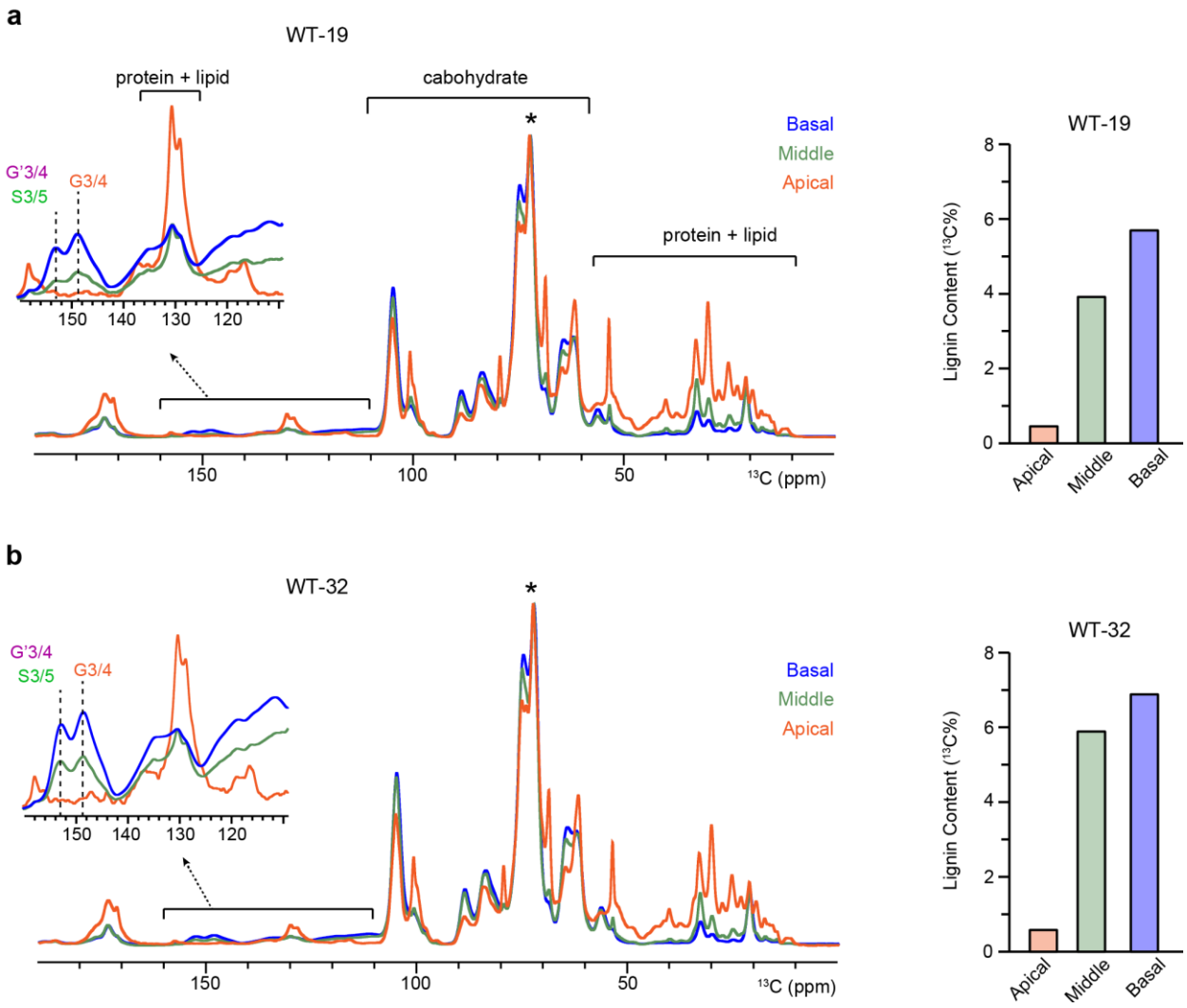

Supplementary Figure 6. Lignification of WT *Arabidopsis* across the whole inflorescence. 1D CP spectra collected from three different inflorescence regions were compared for the WT *Arabidopsis* grew to heights of 19 cm (**a**) and 32 cm (**b**). All spectra are normalized with respect to the highest carbohydrate peak (asterisk). The zoomed-in region shows the difference in the overall lignin content between different inflorescence regions. For both 19 cm and 32 cm samples, the unique lignin peaks at 152.5 ppm (S3/5, G'3/4) and 148.5 ppm (G3/4) are depleted in the apical segment (orange), whereas the aromatic residue and lipid peaks became prominent and dominant. The overall lignin content in the rigid fraction of whole cell estimated from the 1D CP spectra are shown on the right. Source data are provided as a Source Data file.

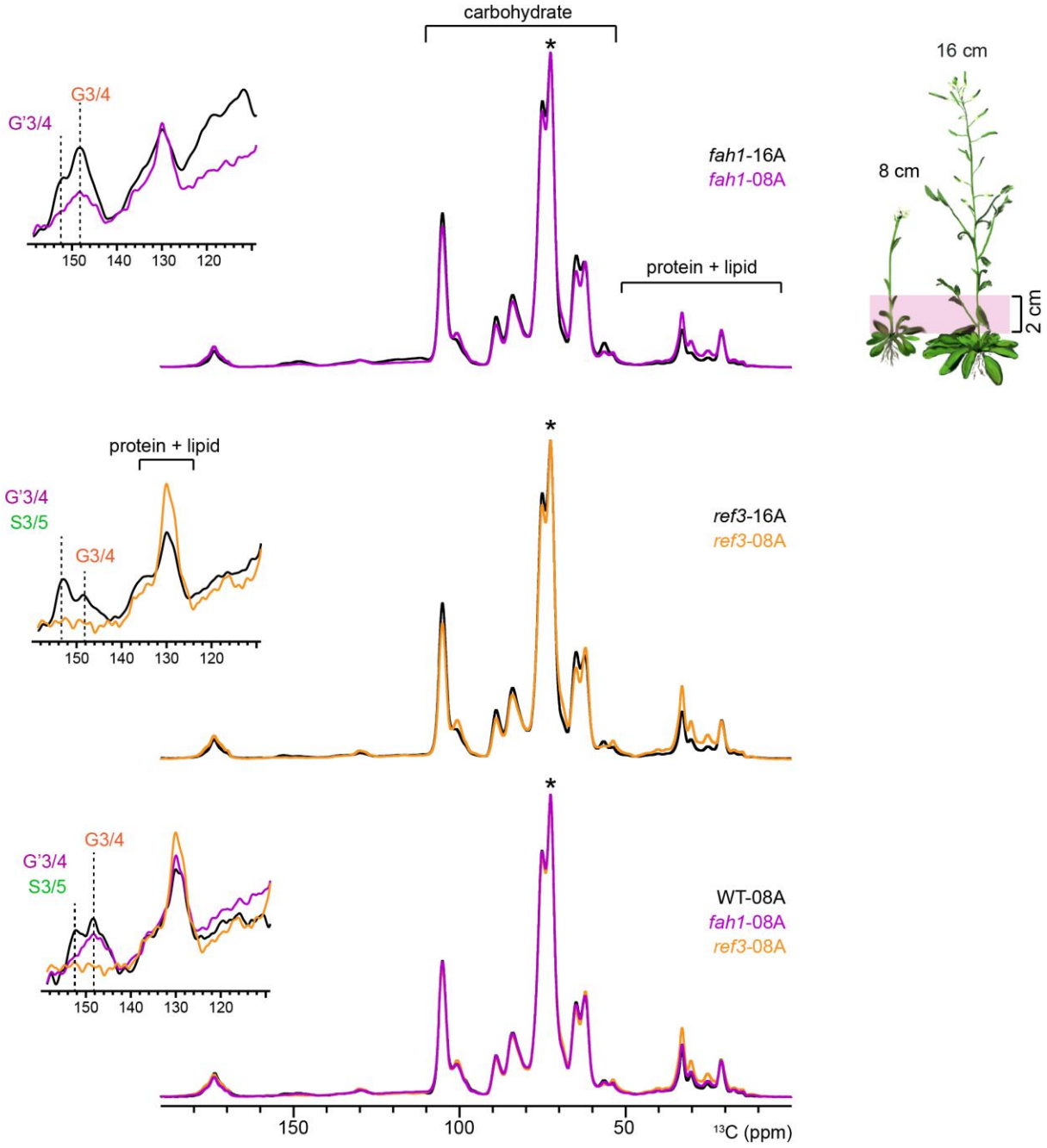

Supplementary Figure 7. Comparison of lignin signals in mutants at different growth stages. 1D CP spectra were collected on the basal segment A (0-2 cm) from inflorescences grown to heights of 8 cm and 16 cm, including the two mutants *fah1-2* and *ref3-3*, referred to as *fah1*-08/16A and *ref3*-08/16A, respectively. The 1D CP spectrum from WT 08A is also included in the overlay as a reference. All spectra are normalized with respect to the highest carbohydrate peak (asterisk). The zoomed-in region shows the difference in the lignin content, with the unique lignin peaks indicated by dashed lines. The unique lignin peaks are depleted in the *ref3*-08A sample, and the peak at around 130 ppm is dominated by aromatic residue and lipid signals. The protein and lipid signals in the 10-50 ppm region are also more prominent for the *ref3*-08A sample.

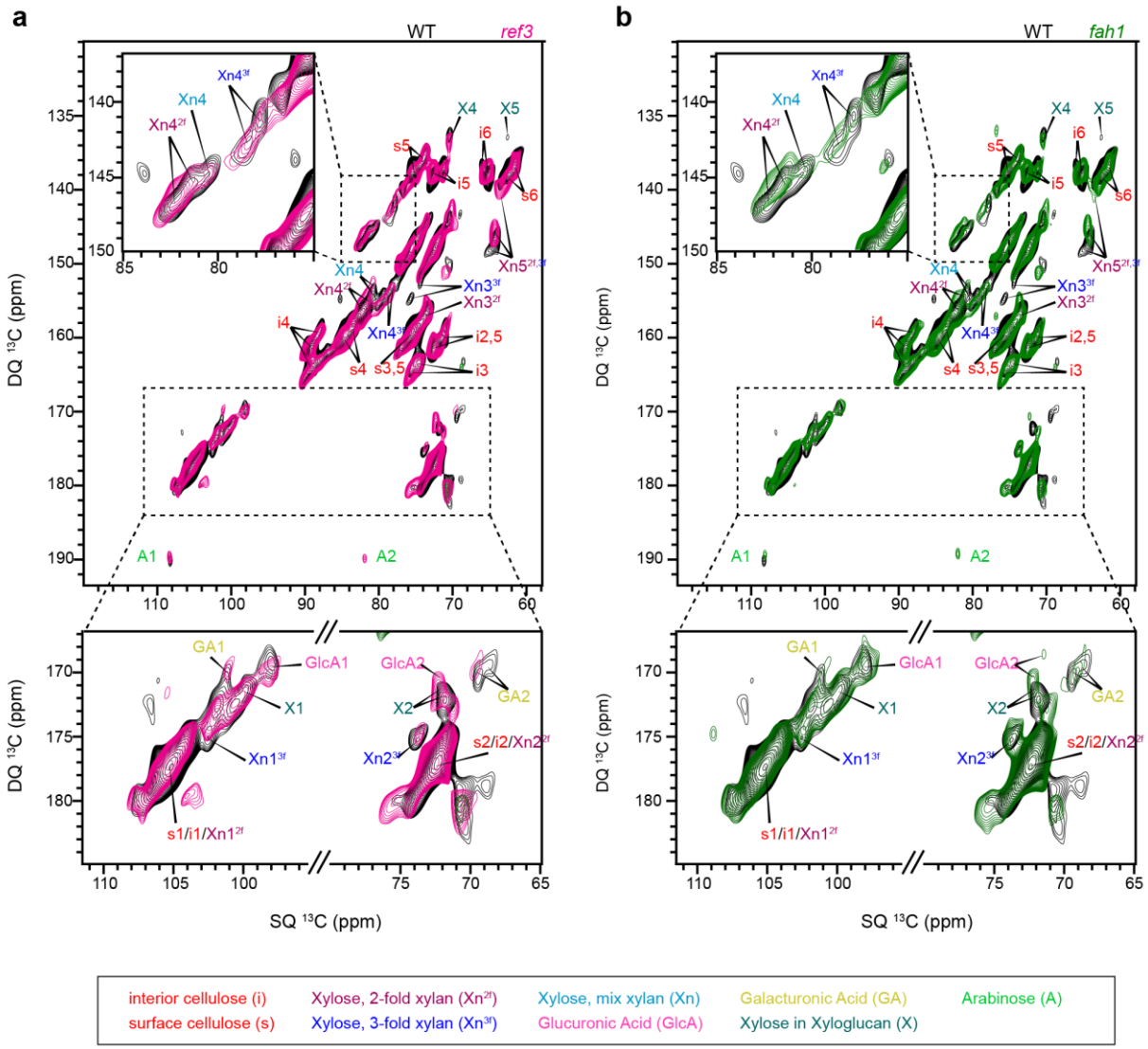

Supplementary Figure 8. Carbohydrate regions of CP J-INADEQUATE spectra. Overlayed spectra are shown for (**a**) WT-16A and *ref3*-16A, and for (**b**) WT-16A and *fah1*-16A. Spectra for each sample were plotted using different base contour levels such that the main peak contours appear at comparable intensities. Boxed regions were enlarged and displayed in additional panels, where contour levels were lowered to better highlight peak patterns in these regions.

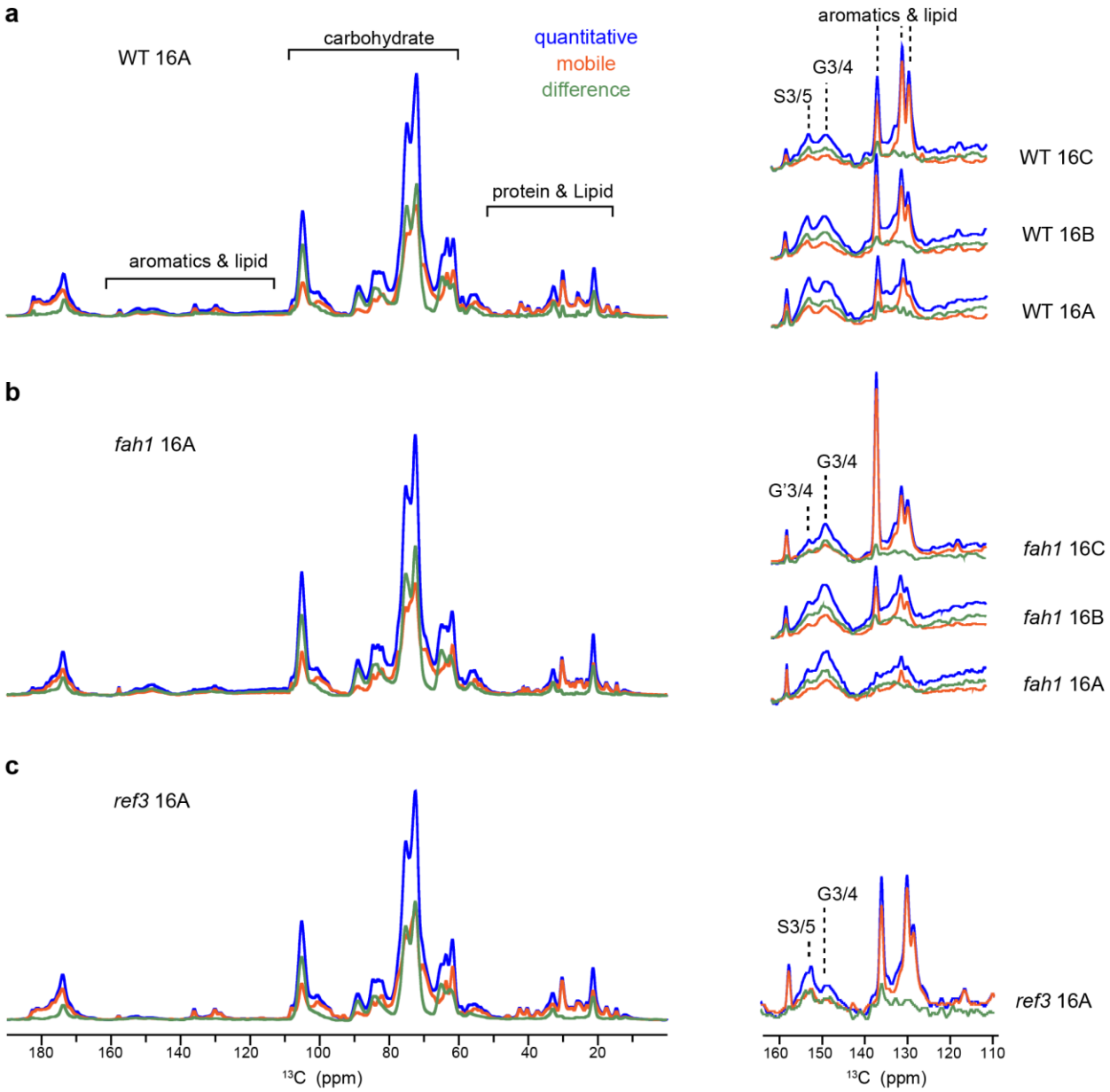

Supplementary Figure 9. 1D ^{13}C DP spectra for WT and mutants of *Arabidopsis*. 1D ^{13}C DP spectra are overlaid for different segments of (**a**) WT, (**b**) *fah1* and (**c**) *ref3*. The spectra in blue have a long recycle delay of 35 s showing quantitative ^{13}C composition. The spectra in red have a recycle delay of 2 s showing ^{13}C species that are relatively more mobile and do not show up in the 1D CP spectra. The spectra in green show the difference between the two types of DP spectra, indicating relatively rigid fractions. The panels on the right display zoomed-in view of the region that include lignin aromatic carbons, fatty acyl chain carbons in lipids, and sidechain carbons of aromatic amino acid residues. The blue spectra on the right were normalized with respect to the highest carbohydrate peak at 72.5 ppm (not shown here) for each sample, and the red and green spectra were scaled according to their respective normalization factors. The strong sharp peaks at 136, 130, and 128.5 ppm in the zoomed-in region arise from the protein and lipid signals which are largely dynamic, and they grow stronger in higher segments from segment A to C. The lignin peaks are at around 152.5 ppm (S3/5, G'3/4) and 148.5 ppm (G3/4) and are mostly in the rigid fraction (green), apart from the *fah1*-16C and *ref3*-16A samples.

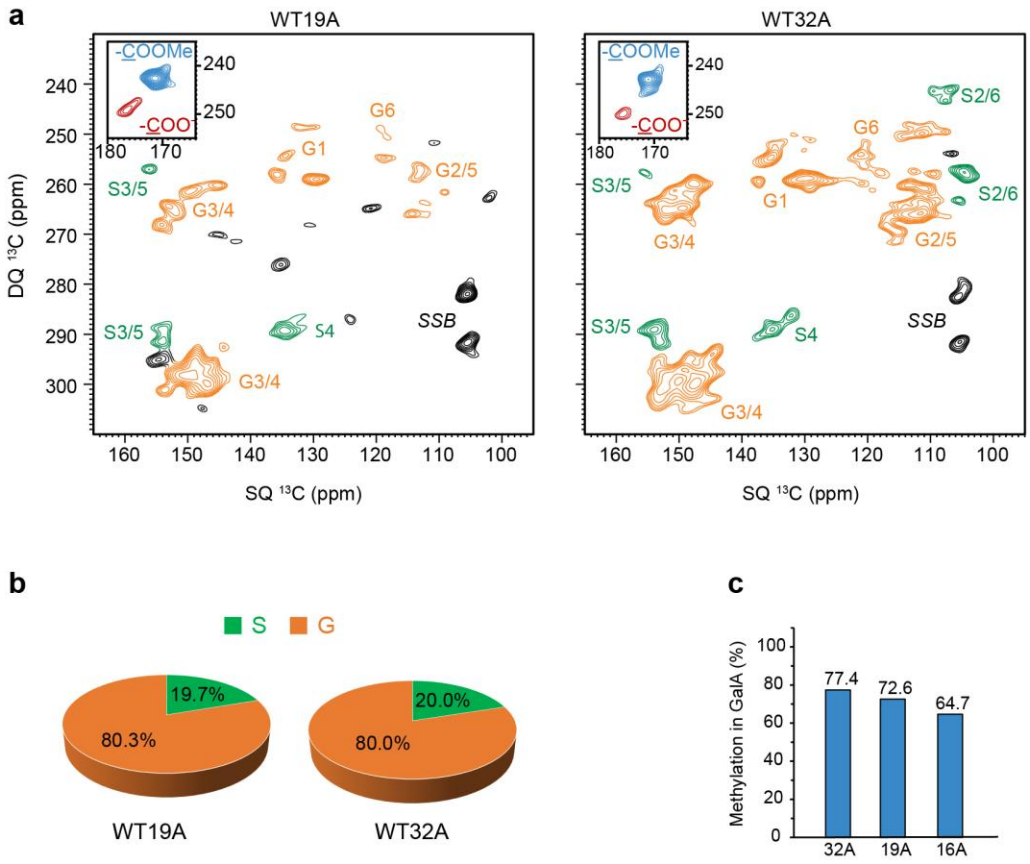

Supplementary Figure 10. Additional CP J-INADEQUATE spectra of wild-type stems. (**a**) CP-based J-INADEQUATE spectra collected on WT-19A (left) and WT-32A (right). The S and G lignin peaks are colored in green and orange, respectively. The inset shows the C6 peak region of GalA, with unmethylated in red and methylated in blue. The peaks in region 100 – 110 ppm (SQ)/ 280 – 295 ppm (DQ) are spinning sideband (SSB). (**b**) The S/G unit ratio in each sample. Estimations were based on the peak volumes corresponding to carbon 3/5 and 4 of the S units, and carbon 3/4 signals of the G units. (**c**) Methylation level of GalA in each sample. The molar fraction of methylated GalA was estimated by comparing the peak volumes of two carbonyl peaks corresponding to methylated and unmethylated GalA units shown in the inset of panel (a). The WT-16A data was also included here as a reference. Source data are provided as a Source Data file.

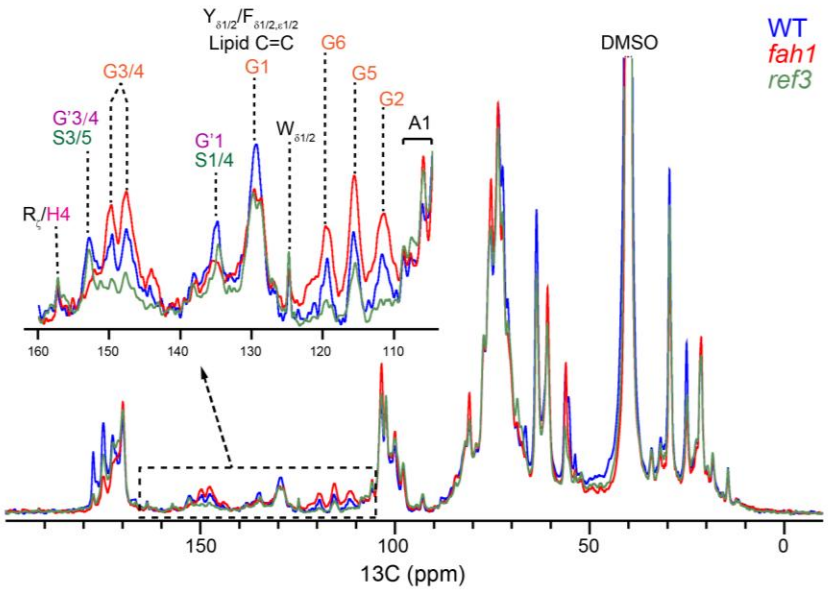

Supplementary Figure 11. 1D solution NMR spectra of *Arabidopsis* WT and mutants. 1D DP ^{13}C spectra of the three samples dissolved in DMSO-d_6. All spectra are normalized to the integration of the main carbohydrate region (110-65 ppm). The DMSO solvent peaks are about 25 folds of the carbohydrate peaks and are cut off from the spectra. The inset zooms in at the aromatic region showing differences between the samples. A: arabinose; F: phenylalanine; Y: tyrosine; W: tryptophan; R: asparagine.

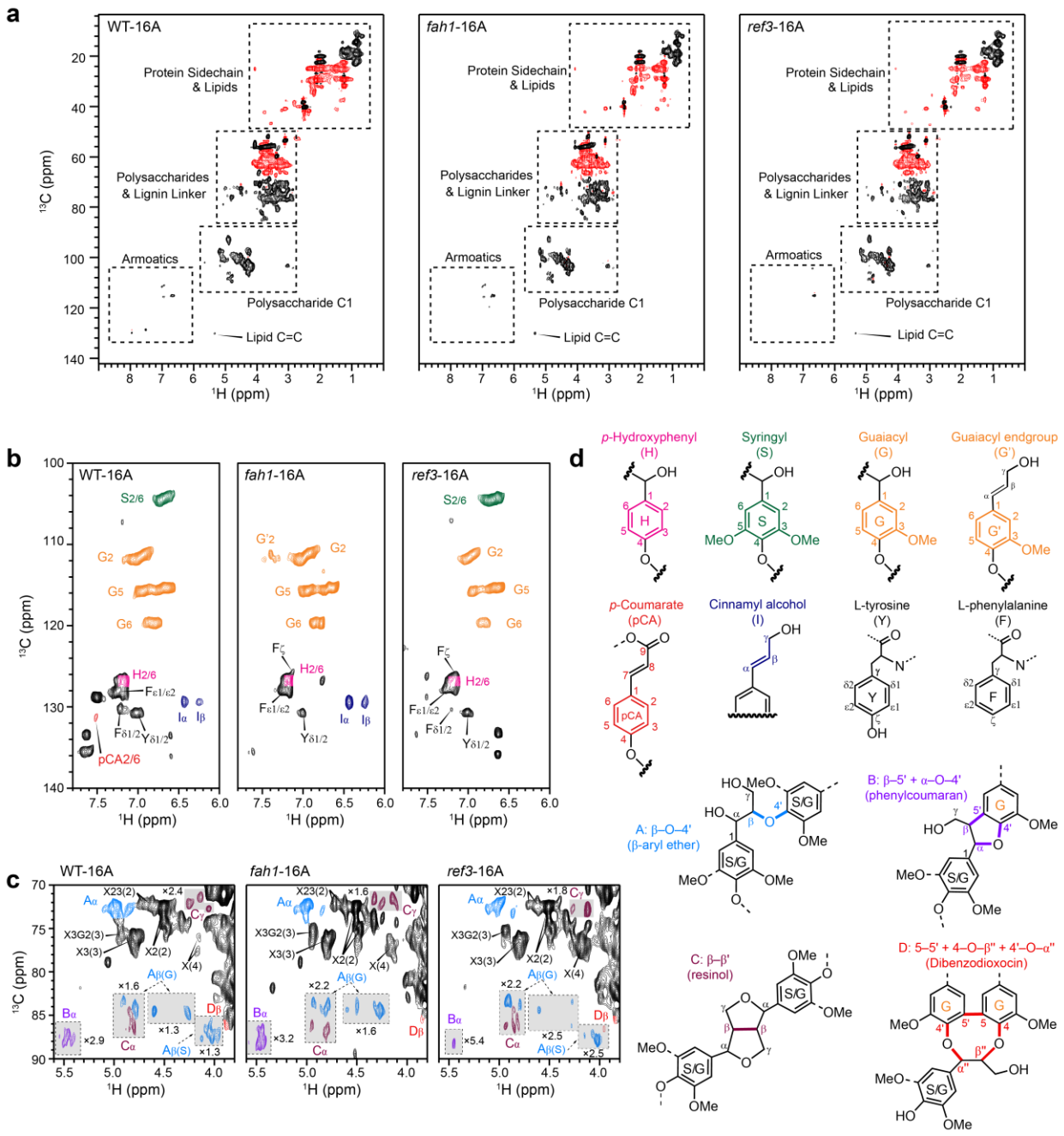

Supplementary Figure 12. Solution NMR spectra of *Arabidopsis* WT and mutants. 2D ^{1}H-^{13}C HSQC spectra are shown as **(a)** full spectra, **(b)** lignin aromatic region and **(c)** lignin linkage region. Lignin peaks are color-coded with structures presented in **(d)**. In panel **(a),** Different peak regions are indicated with dashed boxes. CH and CH_3 peaks are in black and CH_2 peaks are in red. In **(b)**, the base contour levels are lower than that in **(a)** to emphasize the weaker lignin peaks. Phenylalanine (F) and tyrosine (Y) are also detected and labeled. In **(c)**, shaded regions are plotted at different contour levels to emphasize the weaker peaks, with the magnification factors given. A_β(S) and A_β(G) indicate the 4' in the β-O-4' link belongs to S and G unit, respectively.

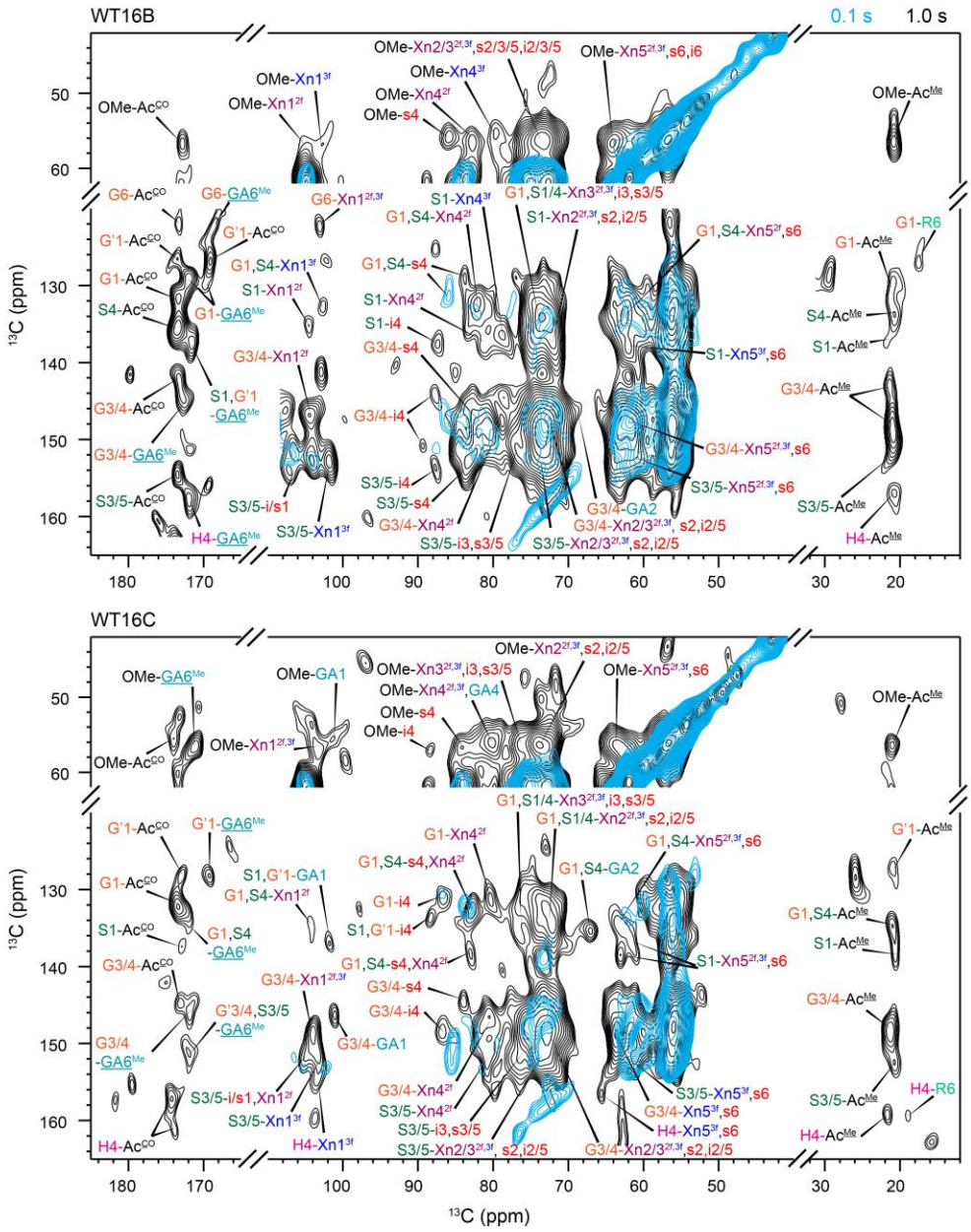

Supplementary Figure 13. 2D ^{13}C-^{13}C correlation spectra of wild-type samples. For each sample, the spectra were measured using short (0.1 s; blue) and long (1.0 s; black) mixing times. The short-range and long-range spectra were plotted at different base contour levels, in such a way that the main diagonal peaks of each spectrum are at similar levels. Data are shown for WT 16B (top) and WT 16C (bottom) samples. Only lignin-carbohydrate cross-peak are labeled. In addition to lignin-xylan and lignin-cellulose interactions, interactions between lignin and pectin can also be observed, for example, carbon sites of methylated GalA (GA6^{Me}, 168-172 ppm) and unmethylated GalA (GA6, 175.5-177.5 ppm), C1 and C2 of GalA (GA1 at 99.5-101.5 ppm and GA2 at 67-69 ppm), and C6 of rhamnose (R6, 17-19 ppm).

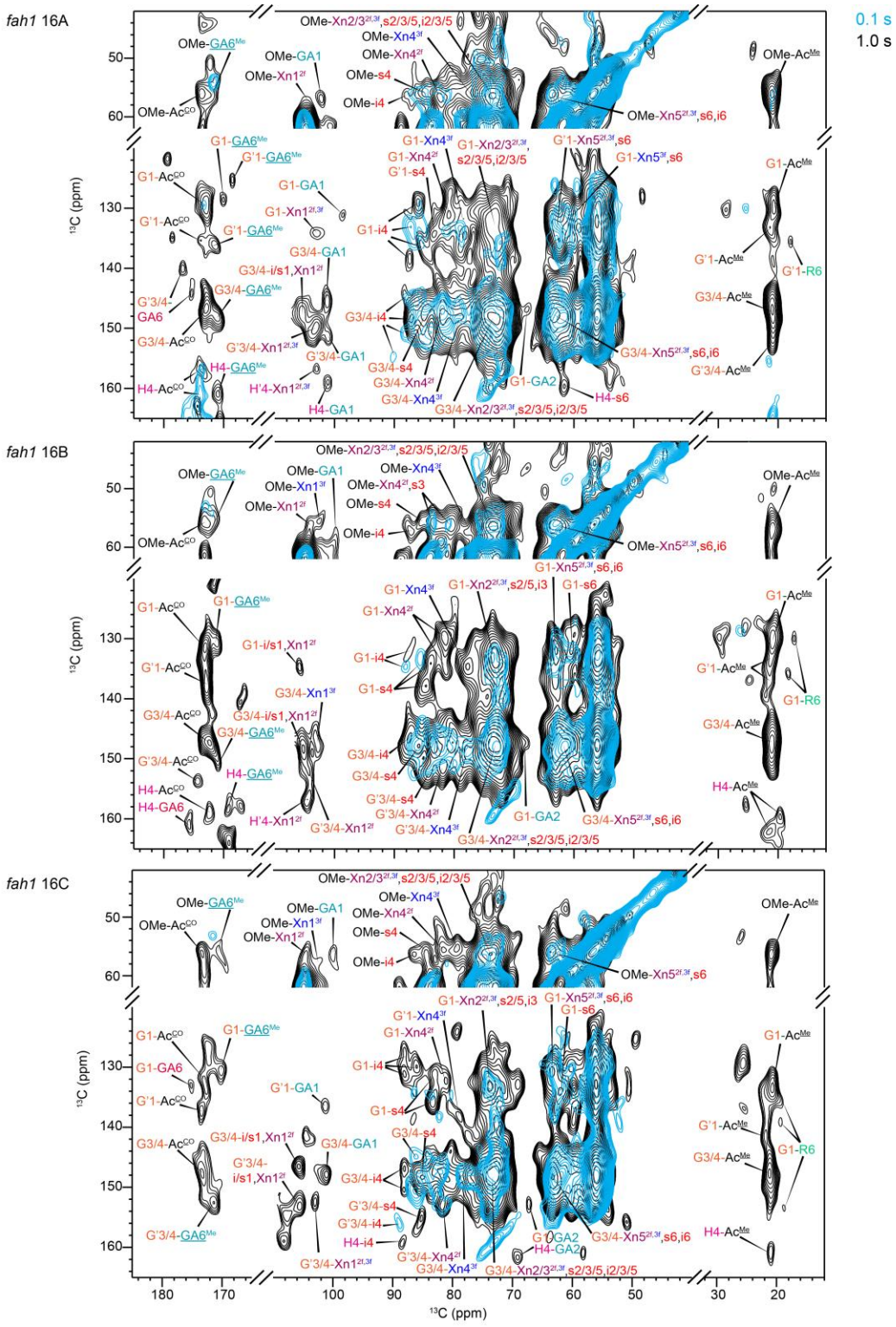

Supplementary Figure 14. 2D ^{13}C-^{13}C correlation spectra of *fah1* samples. For each sample, the spectra were measured using short (0.1 s; blue) and long (1.0 s; black) mixing times. Data are shown for *fah1*-16A (top), *fah1*-16B (middle), and *fah1*-16C (bottom). The short-range and long-range spectra were plotted at different base contour levels, in such a way that the main diagonal peaks of each spectrum are at similar levels. Only lignin-carbohydrate cross-peak are labeled.

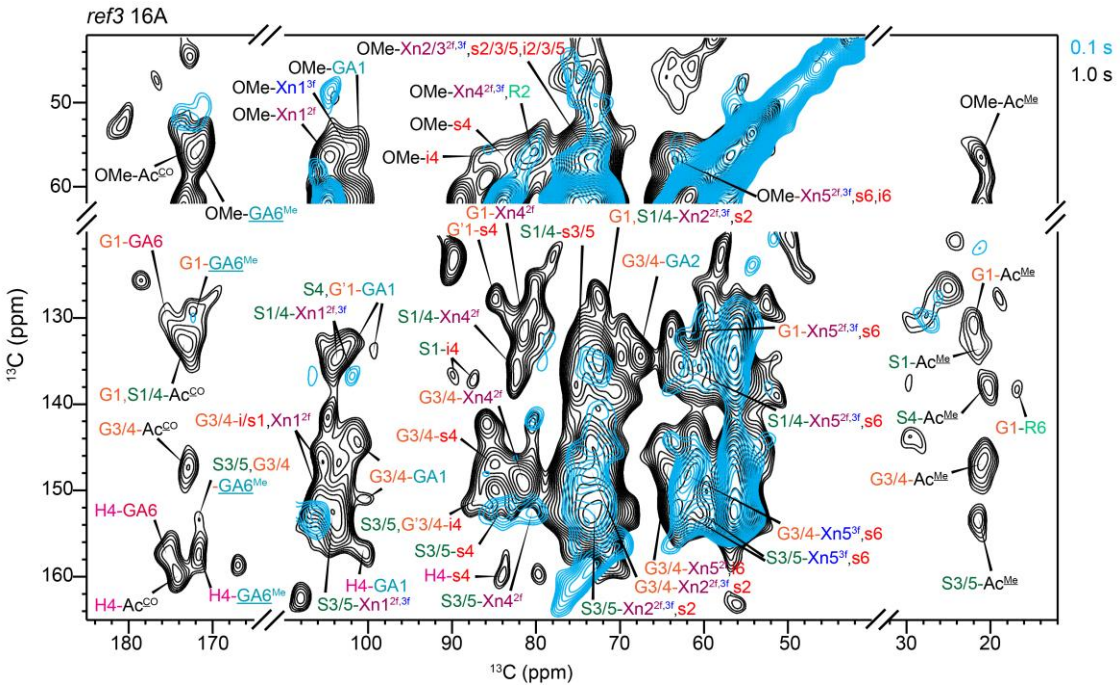

Supplementary Figure 15. 2D ^{13}C-^{13}C correlation spectra of *ref3*-16A sample. The spectra were measured using short (0.1 s; blue) and long (1.0 s; black) mixing times. The short-range and long-range spectra were plotted at different base contour levels, in such a way that the main diagonal peaks of each spectrum are at similar levels. Only lignin-carbohydrate cross-peak are labeled.

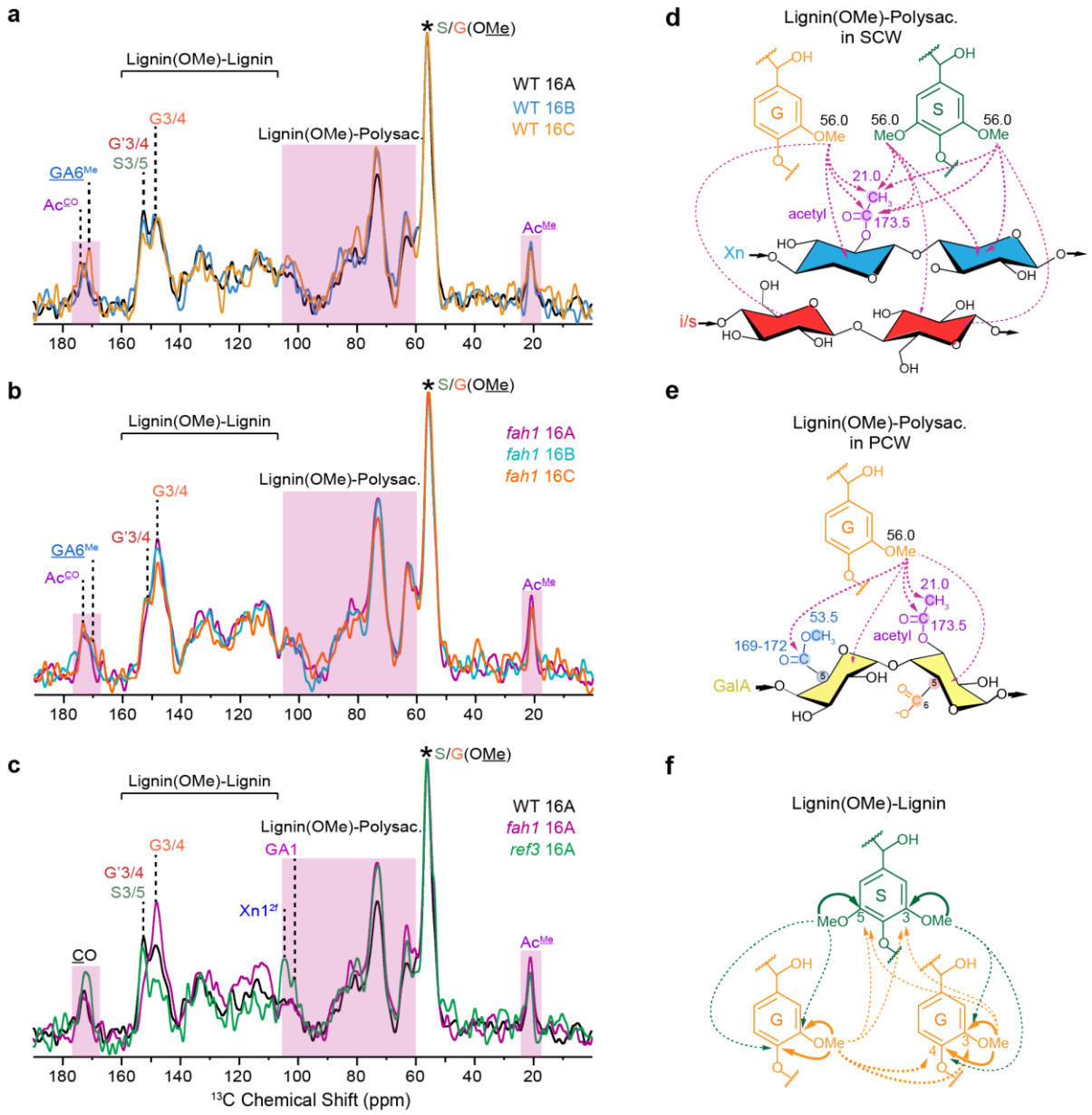

Supplementary Figure 16. Intermolecular interactions viewed from 1D cross sections. (a-c) 1D cross-sections extracted at 56 ppm (OMe) from 2D dipolar-gated PDSD spectra normalized by the OMe peak (asterisk). Lignin-carbohydrate interaction regions are highlighted in pink. Various carbonyl sites, i.e., acetyl groups (Ac^{CO}, 173.5 ppm) and methylated GalA C6 ($GA6^{Me}$, 171 ppm), are observed in the basal segment C of WT and *fah1*. Strong interactions of lignin with xylan ($Xn1^{2f}$, 104.5 ppm) and with pectin (GA1, 100.5 ppm) are observed in *ref3*-16A. (**d-f**) Structural representation of interactions observed in 1D slices. Inter- and intramolecular interactions are indicated by dashed lines and solid lines with arrows, respectively. (**d**) Interactions between lignin OMe groups and cellulose/xylan carbons. (**e**) Interactions between lignin OMe groups and pectin, including C1-C5 of GalA (GA), acetyl carbons of GalA, and methyl esters ($GA6^{Me}$, 171 ppm) from methylated GalA. (**f**) Interactions between lignin OMe groups and lignin aromatic carbon sites. Solid lines indicate the nearest intramolecular interactions, giving rise to the most prominent lignin aromatic carbon peaks in the 1D slices, G3/4 and S3/5. Signals from neighboring lignin units and those further away contribute to these peaks to a lesser extent and are indicated by dashed lines.

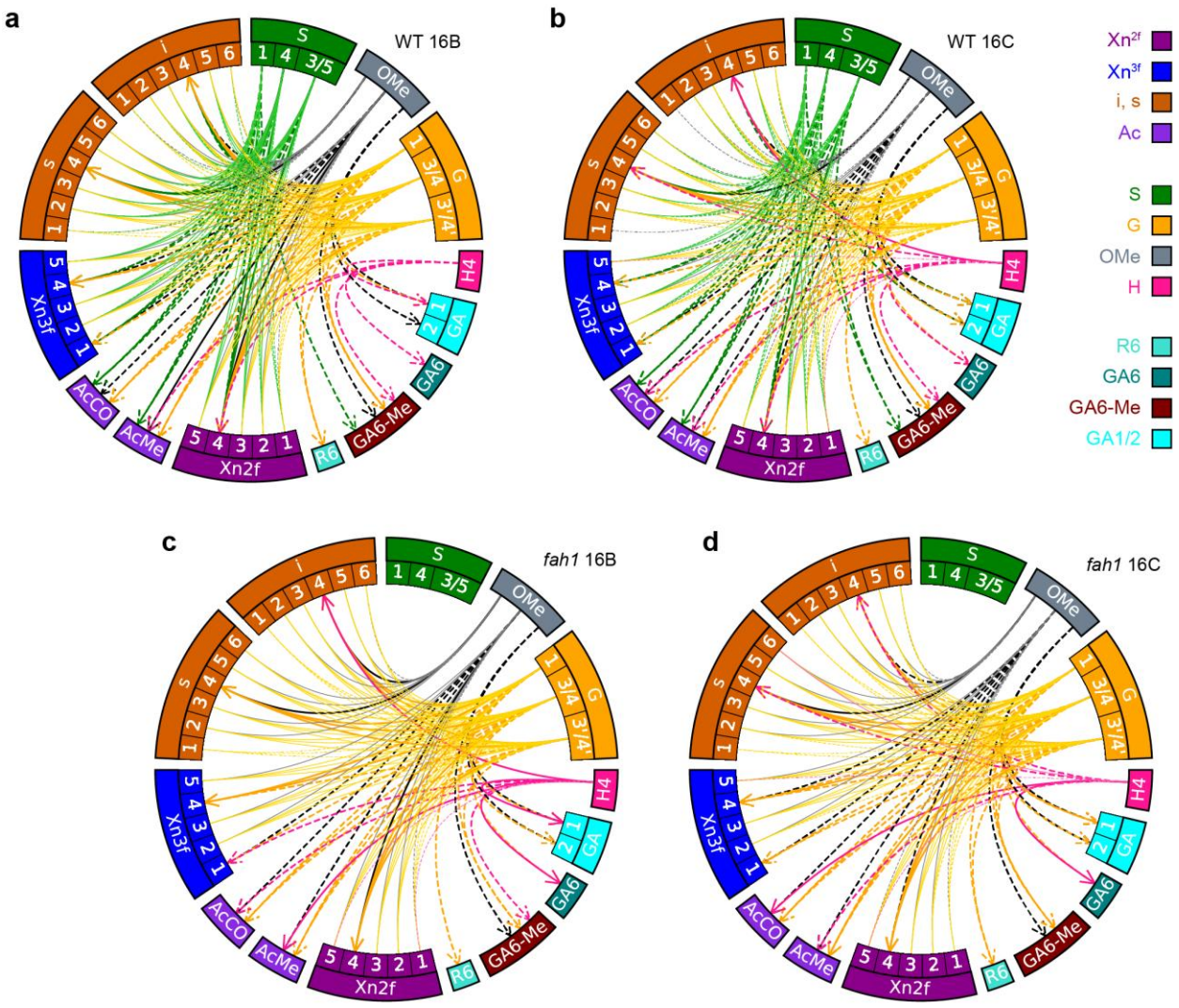

Supplementary Figure 17. Chord diagram for intermolecular interactions. The interactions were based on cross-peaks identified in the 2D dipolar-gated ^{13}C-^{13}C correlation spectra for samples (**a**) WT16B, (**b**) WT16C, (**c**) *fah1*-16B, and (**d**) *fah1*-16C. The carbon sites are color-coded with the legends on the right. Solid lines and dashed lines represent cross-peaks identified in the short-range and long-range spectra, respectively. Thick lines with arrow indicate unambiguous, site-specific cross-links and narrow lines without arrow indicate convoluted cross-links. The diagrams were compiled using pyCirclize script (https://github.com/moshi4/pyCirclize). Source data are provided as a Source Data file.

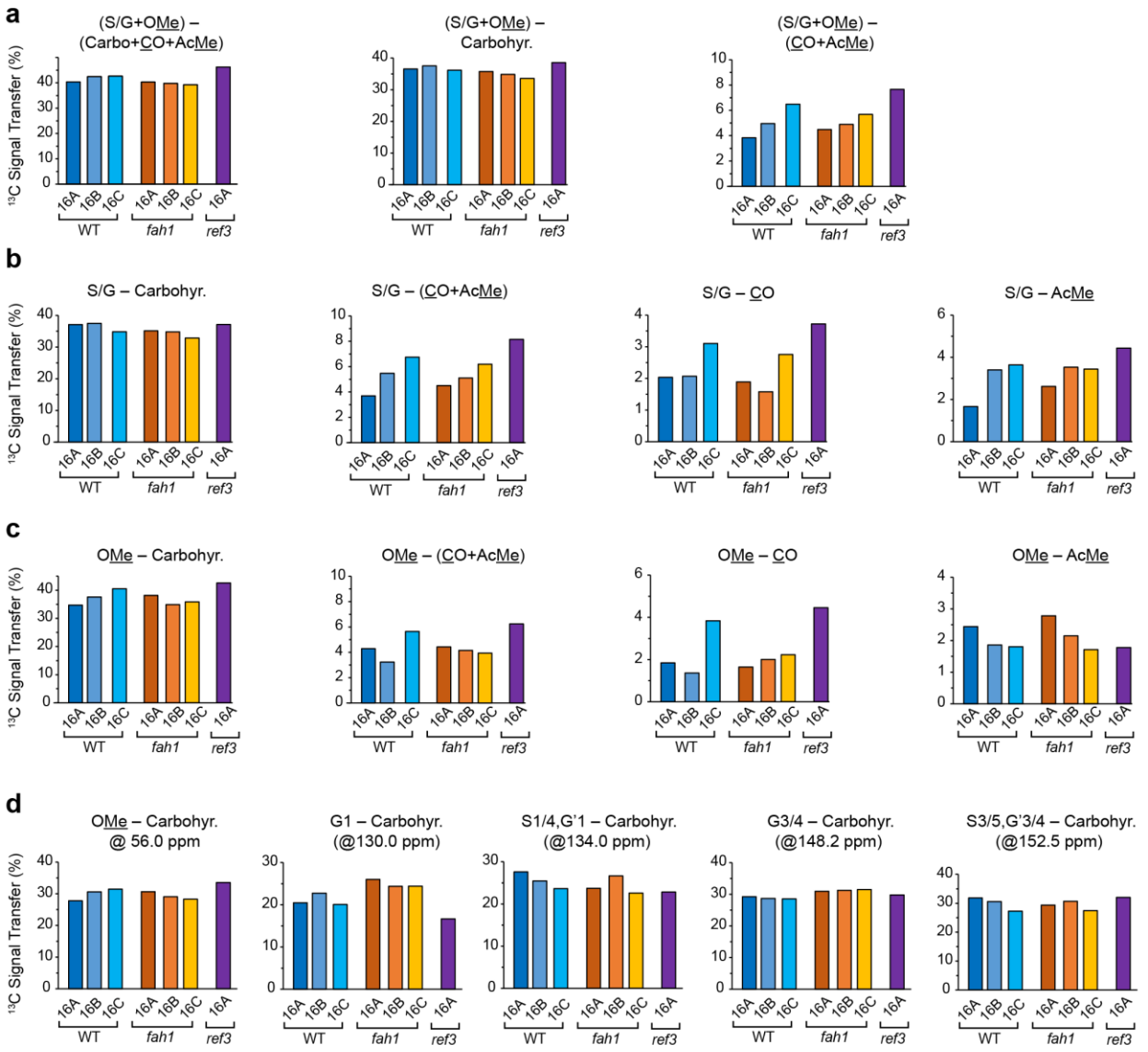

Supplementary Figure 18. Lignin-carbohydrate interactions presented as bar charts. Bar charts show the percentage carbon signals transferred from lignin to carbohydrate, analyzed from dipolar-gated PDSD spectra (1 s mixing time, long-range). The lignin-carbohydrate interactions were analyzed in four different categories: the overall lignin-carbohydrate contacts that include both S/G and OMe carbons (**a**), the transfer that only from S/G carbons (**b**) and OMe carbons (**c**), respectively, and the transfer from specific carbon sites analyzed from 1D cross-sections (**d**). S/G: deprotonated lignin carbons; OMe: lignin methoxy carbons; carbo: carbohydrate carbons with acetyls excluded; Ac: acetyl methyl and carbonyl carbons; AcMe: methyl carbons from acetyl group; CO: carbonyl carbons, including those from acetyl and C6 of GalA. The integration regions for each group are summarized in **Supplementary Table 5**. The resolved lignin carbon sites and their chemical shift values where 1D cross-sections were extracted for the analysis are indicated on top of each chart in panel (**d**). Source data are provided as a Source Data file.

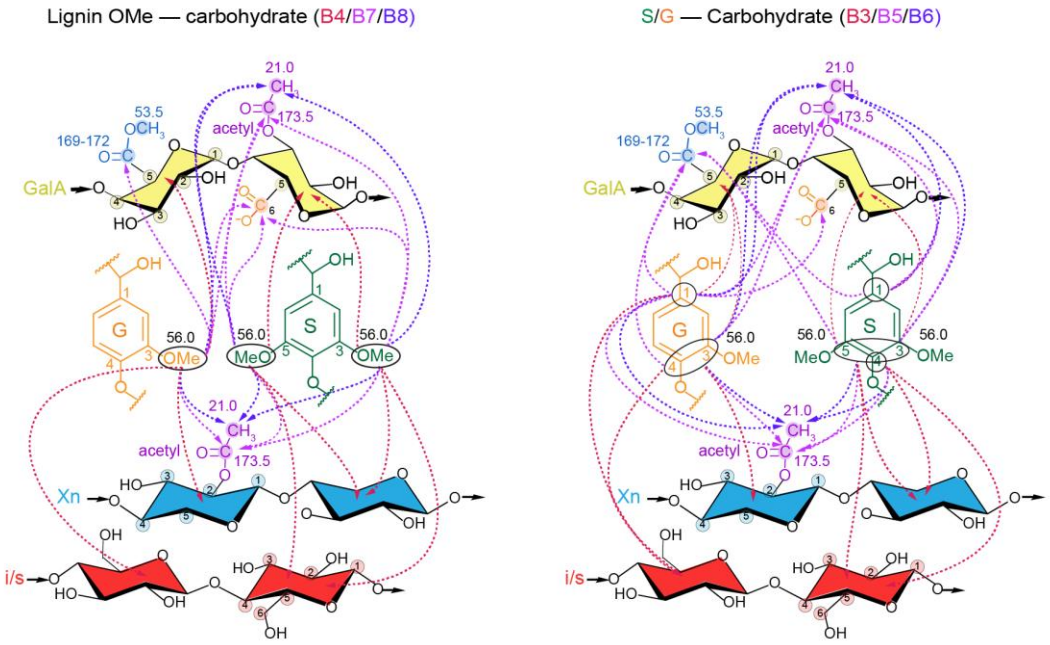

Supplementary Figure 19. Key interactions of lignin OMe and aromatics with carbohydrates. The interactions between lignin OMe and carbohydrates (cellulose: red; xylan: blue; GalA: yellow) are illustrated on the left, corresponding to spectral regions of B4, B7 and B8 listed in **Supplementary Table 5**; the interactions between deprotonated lignin carbons and carbohydrates are on the right, corresponding to spectral regions of B3, B5 and B6.

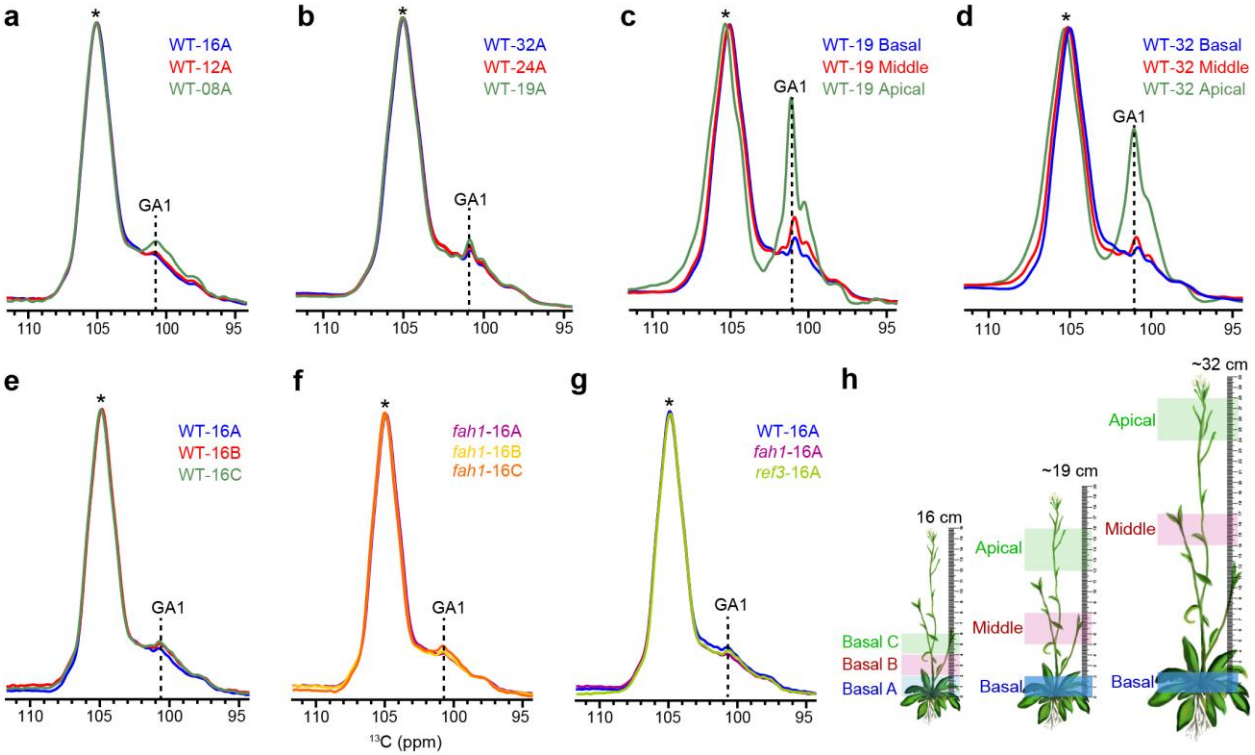

Supplementary Figure 20. Comparison of the rigid pectin signal in all samples. 1D CP spectra are overlayed to show changes of pectin signal in the rigid fraction. Only the C1 peak region of polysaccharides are displayed, in which the pectin signals can be resolved and distinguished from other carbohydrates. All spectra are normalized with respect to the C1 peak of xylan and cellulose (Xn/i/s, asterisk) at around 105 ppm. The C1 peaks of GalA (GA1) at around 100.5 ppm are indicated by dashed lines. (**a**) Comparison between samples WT-16A/12A/08A. (**b**) Comparison between samples WT-32A/24A/19A. (**c**) Comparison between different segments of the WT 19 cm sample. (**d**) Comparison between different segments of the WT 32 cm sample. (**e**) Comparison between samples WT-16A/B/C. (**f**) Comparison between samples *fah1*-16A/B/C. (**g**) Comparison of samples WT16A/*fah1*-16A/*ref3*-16A. (**h**) Illustration of the segments used for each sample.

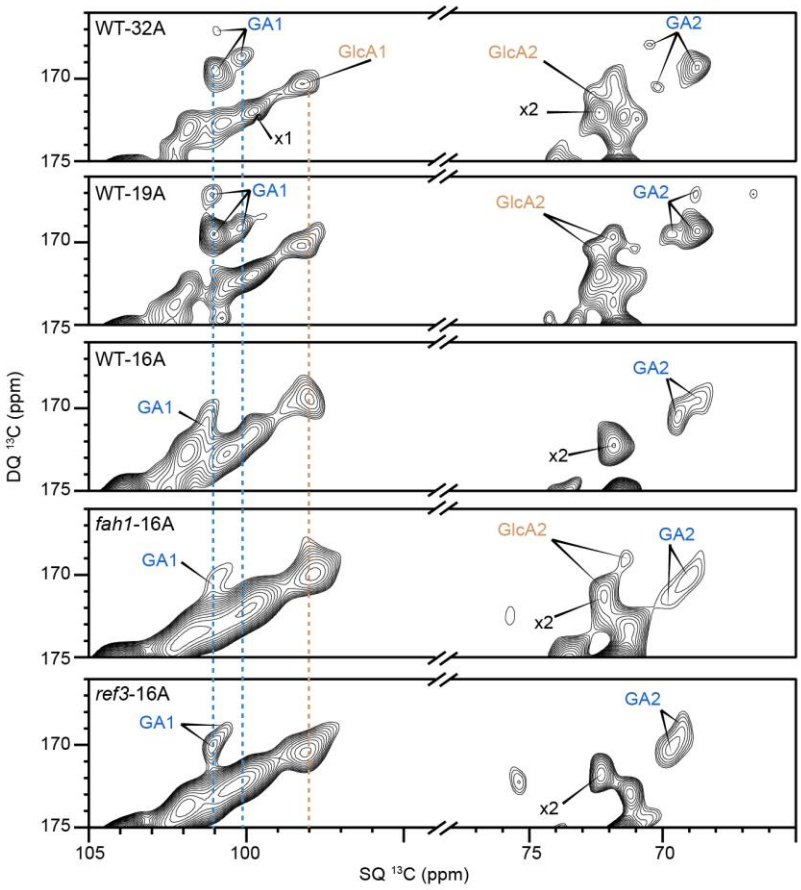

Supplementary Figure 21. Identification of GalA and GlcA signals. C1-C2 region of CP-based refocused J-INADEQUATE spectra showing signals of GalA (GA) and GlcA for samples of WT-32A, WT-19A, WT-16A, *fah1*-16A and *ref3*-16A. The main GA1 SQ chemical shifts (101.5-99.5 ppm) are indicated by the blue dashed lines, which partially overlap with that of xylose (x1) units in xyloglucan. The GlcA1 SQ chemical shift (98 ppm) is indicated by the brown dashed line.

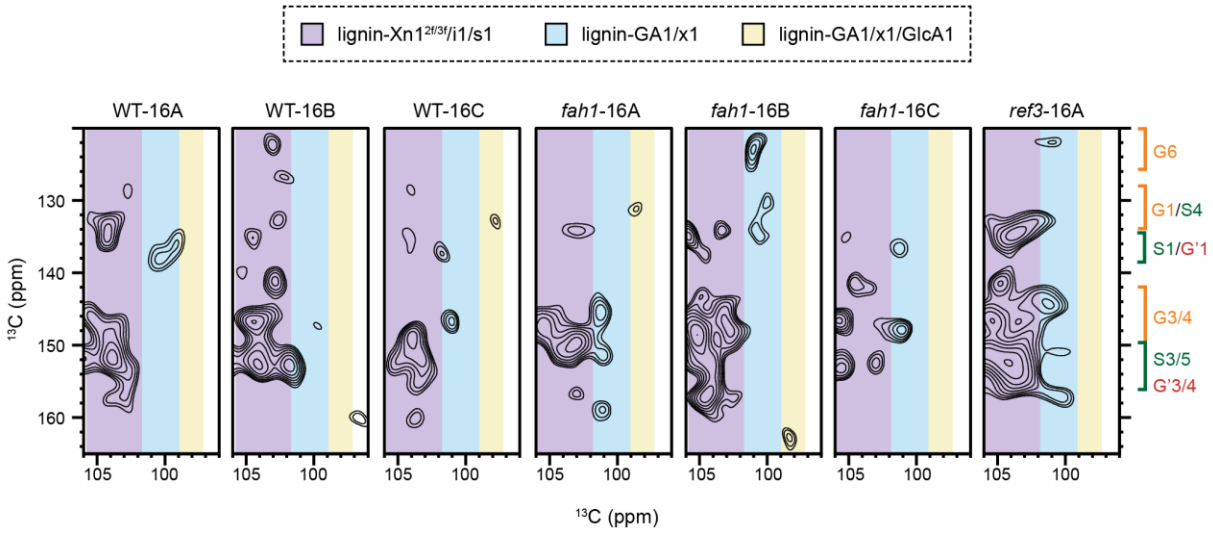

Supplementary Figure 22. Absence of lignin-GlcA cross-peaks. Spectral regions of gated long-range ^{13}C-^{13}C correlation spectra show interactions between lignin aromatic carbons and various C1 sites. The purple band indicates lignin interactions with xylan and cellulose. The blue band highlights lignin interactions with pectin, with potential mixed contributions from xyloglucan. The yellow band highlights lignin interactions with GlcA, with potential contributions from minor species of GA1 and x1, where no prominent interactions are observed.

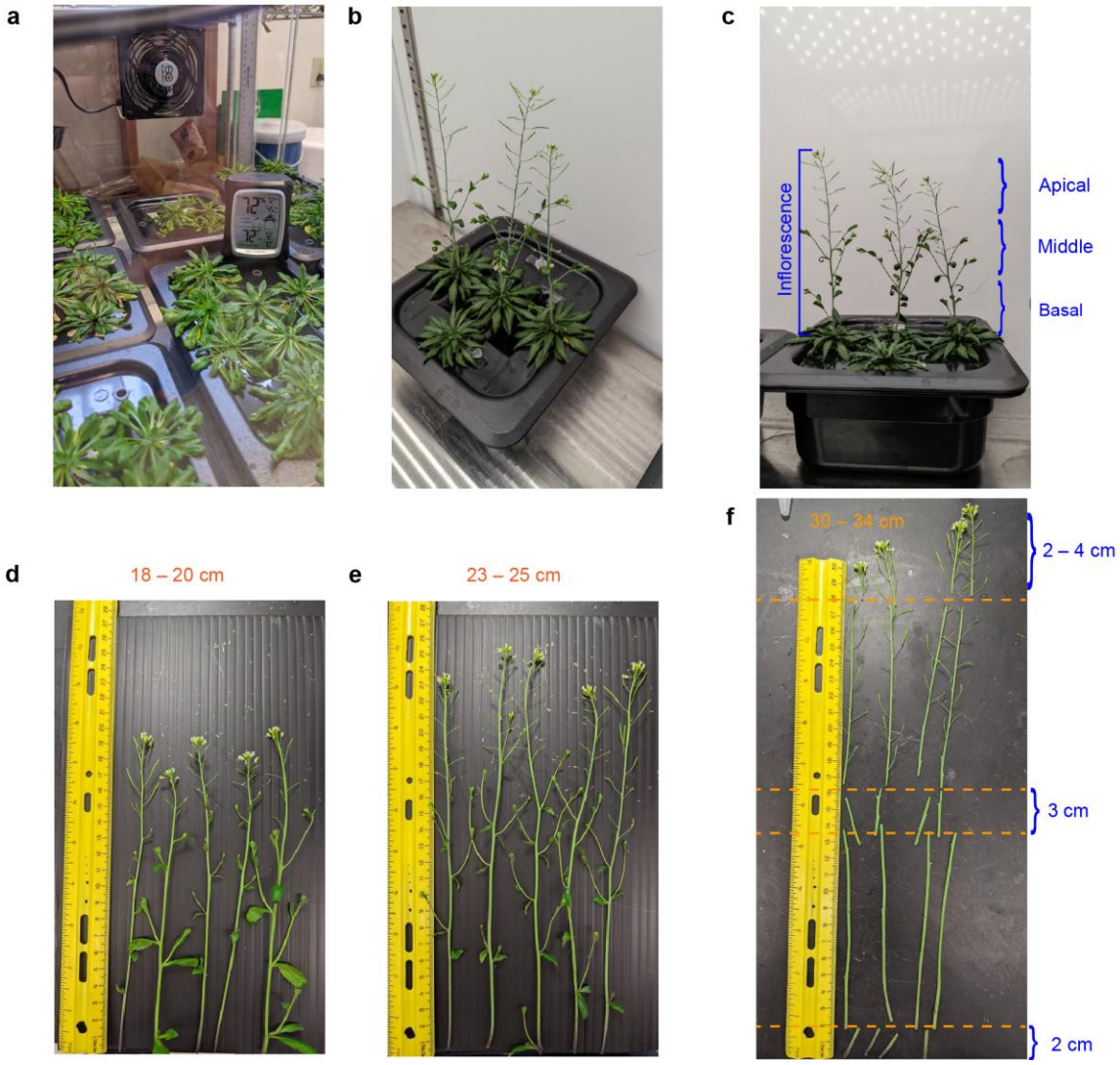

Supplementary Figure 23. Illustrations of *Arabidopsis* stem sample preparation. (**a**) Hydroponic Growth of *Arabidopsis*. (**b-c**) Top view and side view of *Arabidopsis* inflorescence, respectively. The basal, middle and apical regions are indicated on the right. (**d-f**) Photographs of *Arabidopsis* stems harvested at different growth stages, with the lengths of the stems indicated at the top. (**f**) shows an example of how different regions of stems were cut for preparing the samples used in the NMR experiments.

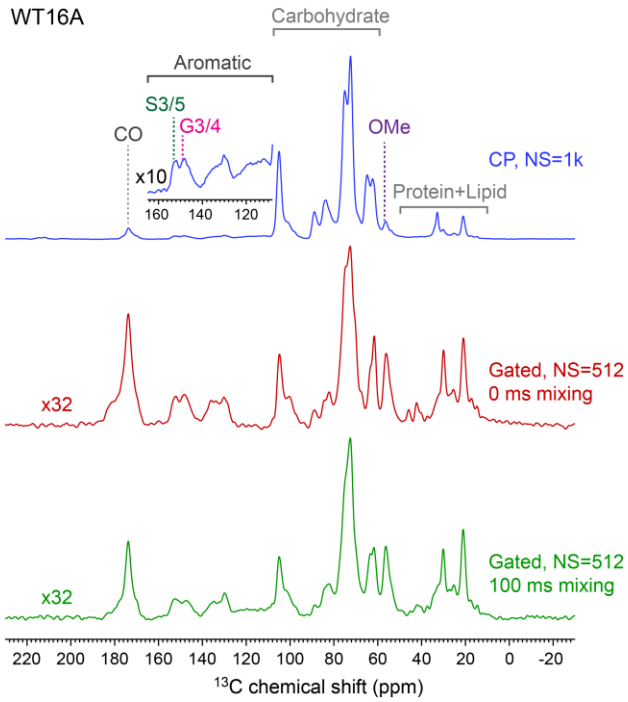

Supplementary Figure 24. 1D spectra showing the effect of dipolar gating. Top row is the 1D CP experiment without the dipolar-gating step, in which the carbohydrate region is about a hundredfold more intense than the aromatic region; the latter is barely visible without the 10 times magnification in the inset. The middle and bottom rows are the 1D spectra with incorporation of the dipolar-gating step, both of which are scaled up by a factor of 32. The intensity ratio between the carbohydrate region and the aromatic region is attenuated by tenfold in both dipolar-gated spectra.

Supplementary Table 1. Number of intermolecular cross-peaks between carbohydrates and lignin.

	OMe-i/s	OMe - Xn2f	OMe - Xn3f	OMe - Ac(CO+Me)	OMe - pectin	Total # OMe -Carbohydrate
WT16A	10	5	5	2	2	24
WT16B	10	5	5	2	3	25
WT16C	10	5	5	2	3	25
ref3-16A	10	5	5	2	3	25
fah1-16A	8	5	5	2	2	22
fah1-16B	8	5	4	2	3	22
fah1-16C	8	5	5	2	3	23
	# S-i/s	S-Xn2f	S-Xn3f	S-Ac(CO+Me)	S-pectin	Total # S-Carbohydrate
WT16A	23	14	13	6	4	60
WT16B	24	15	14	6	1	60
WT16C	19	14	13	5	4	55
ref3-16A	23	15	15	4	5	62
fah1-16A						
fah1-16B						
fah1-16C						
	# G-i/s	G-Xn2f	G-Xn3f	G-Ac(CO+Me)	G-pectin	Total # G-Carbohydrate
WT16A	24	14	13	5	6	62
WT16B	27	15	12	6	6	66
WT16C	22	15	11	5	7	60
ref3-16A	23	15	12	5	7	62
fah1-16A	26	13	15	5	10	69
fah1-16B	30	15	13	6	4	68
fah1-16C	27	15	14	6	9	71
	# H-i/s	H-Xn2f	H-Xn3f	H-Ac(CO+Me)	H-pectin	Total # H-Carbohydrate
WT16A	2	2	1	1	3	9
WT16B	0	1	0	1	3	5
WT16C	2	2	1	2	3	10
ref3-16A	1	0	1	1	4	7
fah1-16A	2	1	3	1	4	11
fah1-16B	1	2	2	2	3	10
fah1-16C	3	1	0	2	2	8

Supplementary Table 2. The *Arabidopsis* samples for NMR experiments. The short name for each sample is indicated in the bracket after the cut range. When the full height of the inflorescence varies, the average value is given with the range of the length indicated in the bracket.

WT						
Height (cm)	**# of stems**	**Basal Cut Range (cm)**			**Middle Cut Range (cm)**	**Apical Cut Range (cm)**
8	4	0 – 2 (08A)				
12	4	0 – 2 (12A)				
16	3	0 – 2 (16A)	2 – 4 (16B)	4 – 6 (16C)		
19 (18 – 20)	5	0 – 2 (19A)			8 – 11 (19Middle)	16 – 18/20 (19Apical)
24 (23 – 25)	5	0 – 2 (24A)				
32 (30 – 34)	4	0 – 2 (32A)			14 – 17 (19Middle)	28 – 30/30–34 (32Apical)
fah1-2						
Height (cm)	**# of stems**	**Basal Cut Range (cm)**			-	-
8	5	0 – 2 (08A)			-	-
16	2	0 – 2 (16A)	2 – 4 (16B)	4 – 6 (16C)	-	-
ref3-3						
Height (cm)	**# of stems**	**Basal Cut Range (cm)**			-	-
8	5	0 – 2 (08A)			-	-
16	4	0 – 2 (16A)	-	-	-	-

Supplementary Table 3. Solid-state NMR experimental parameters for all samples. T = probe temperature; B_0 = magnetic field; ν_r = MAS frequency; NS = number of scans; d_1 = recycle delay; τ_{HC} = initial $^1H/^{13}C$ CP contact time; t_2/t_1 = acquisition length of direct/indirect dimension; TD2/TD1 = total points of FID for the direct/indirect dimension acquisition; TDeff = effective FID data points used for Fourier transform; LB = line broadening parameter; GB = position of the maximum of the Gaussian function. The 2D acquisition mode for all 2D experiments was States. SPINAL64 ^1H decoupling was used for all experiments at a field strength of 83.3 kHz.

Sample	Experiment	T (K)	B_0 (T)	ν_r (kHz)	NS	d_1 (s)	τ_{HC} (ms)	t_2/t_1 (ms)	TD2/TD1	TDeff	LB (Hz)	GB
WT08A	1D CP	290	9.4	14	1024	2.0	1.0	16.0	1600	-	-40	0.05
	1D DP	298	14.1	14	1024	2.0	-	16.0	1600	-	-10	0.05
WT12A	2D Gated DARR	290	9.4	14	480	1.5	1.0	12.0/2.9	1200/112	500/112	-50/-50	0.05/0.05
	2D Gated PDSD	290	9.4	14	320*2	1.1	1.0	10.2/2.1	1024/80	350/80	-60/-60	0.05/0.05
WT16A	1D CP	298	14.1	14	1024	2.0	1.0	16.0	1600	-	-40	0.05
	1D DP	298	14.1	14	256	35.0, 2.0	-	16.0	1600	-	-10	0.05
	2D Gated DARR	298	14.1	14	320	1.5	1.0	12./3.0	1200/162	600/162	-60/-60	0.05/0.05
	2D Gated PDSD	298	14.1	14	512	1.1	1.0	10.2/2.1	1024/116	600/116	-60/-60	0.05/0.05
	2D CP J-INADEQUATE	275	14.1	18	360*2	1.5	1.9	10.0/3.2	1000/250	300/250	-50/-50	0.05/0.05
WT16B	1D CP	298	14.1	14	1024	2.0	1.0	16.0	1600	-	-40	0.05
	1D DP	298	14.1	14	256	35.0, 2.0	-	16.0	1600	-	-10	0.05
WT16C	2D Gated DARR	298	14.1	14	384	1.5	1.0	12./3.0	1200/162	600/162	-60/-60	0.05/0.05
	2D Gated PDSD	298	14.1	14	512	1.1	1.0	10.2/2.1	1024/116	600/116	-80/-60	0.03/0.05
WT19A	1D CP	293	16.4	20	4096	1.8	1.0	10.0	1250	-	-10	0.05
	1D DP	293	16.4	20	512	35.0	-	16.4	2048	-	-10	0.05
	2D CP J-INADEQUATE	293	16.4	20	64*2	1.8	1.0	12.8/5.2	1600/400	400/270	-50/-50	0.05/0.05
WT19 Middle WT19 Apical	1D CP	293	16.4	20	4096	1.8	1.0	10.0	1250	-	-10	0.05
	1D DP	293	16.4	20	1024	35.0	-	16.4	2048	-	-10	0.05
WT24A	1D CP	293	16.4	20	6144	1.8	1.0	9.7	1024	-	-10	0.05
	1D DP	293	16.4	20	1024	35.0	-	16.4	2048	-	-10	0.05
WT32A	1D CP	293	16.4	20	4096	1.8	1.0	10.0	1250	-	-10	0.05
	1D DP	293	16.4	20	1024	35.0	-	16.4	2048	-	-10	0.05
	2D CP J-INADEQUATE	293	16.4	20	64*2	1.8	1.0	12.8/5.2	1600/400	400/270	-50/-50	0.05/0.05
WT32 Middle WT32 Apical	1D CP	293	16.4	20	4096	1.8	1.0	10.0	1250	-	-10	0.05
	1D DP	293	16.4	20	1024	35.0	-	16.4	2048	-	-10	0.05
fah1 08A	1D CP	290	9.4	14	1024	2.0	1.0	16	1600	-	-10	0.05
fah1 16A	1D CP	298	14.1	14	1024	2.0	1.0	16.0	1600	-	-40	0.05
	1D DP	298	14.1	14	256	35.0, 2.0	-	16.0	1600	-	-10	0.05
	2D Gated DARR	298	14.1	14	384	1.5	1.0	12./3.0	1200/162	600/162	-60/-60	0.05/0.05
	2D Gated PDSD	298	14.1	14	512	1.1	1.0	10.2/2.1	1024/116	600/116	-80/-60	0.03/0.05
	2D CP J-INADEQUATE	275	14.1	18	360*2	1.5	2.1	10.0/3.2	1000/250	400/250	-50/-50	0.05/0.05
fah1 16B *fah1* 16C	1D CP	298	14.1	14	1024	2.0	1.0	16.0	1600	-	-40	0.05
	1D DP	298	14.1	14	256	35.0, 2.0	-	16.0	1600	-	-10	0.05
	2D Gated DARR	298	14.1	14	384	1.5	1.0	12./3.0	1200/162	600/162	-60/-60	0.05/0.05
	2D Gated PDSD	298	14.1	14	512	1.1	1.0	10.2/2.1	1024/116	600/116	-80/-60	0.03/0.05
ref3 08A	1D CP	290	9.4	14	1024	2.0	1.0	16	1600	-	-10	0.05
ref3 16A	1D CP	298	14.1	14	1024	2.0	1.0	16.0	1600	-	-40	0.05
	1D DP	298	14.1	14	256	35.0, 2.0	-	16.0	1600	-	-10	0.05
	2D Gated DARR	298	14.1	14	384	1.5	1.0	12./3.0	1200/162	800/162	-60/-60	0.05/0.05
	2D Gated PDSD	298	14.1	14	512	1.1	1.0	10.2/2.1	1024/116	400/116	-80/-80	0.03/0.03

	2D CP J-INADEQUATE	275	14.1	18	360*2	1.5	2.0	10.0/3.2	1000/250	400/250	-50/-50	0.05/0.05

Supplementary Table 4. ^{13}C chemical shifts of lignin on TMS scale. Unidentified site is indicated as "-". Degenerate sites are separated by "/".

	G						S					
Sample	C1	C2	C3*	C4*	C5	C6	C1	C2	C3	C4	C5	C6
WT-16A	134.8	111.2	147.6	144.0	110.9	118.8	138.3	105.5	152.8	134.5	152.8	105.5
	134.8/136.9	112.0	148.7	145.6	115.5/117.2	-	135.5	104.3	153.9	133.1	153.9	104.3
	133.4	111.4/109.5	152.4	146.6	115.5/117.2	-						
	130.5	114.2	151.1	148.5	116.5	-						
WT-19A	131.8	112.5	148.5	144.6	115.6	-	135.3	108.6	153.5	135.2	153.5	108.6
	131.8	112.6	149.2	145.8	114.1	121.9	135.3	108.3	154.1	137.3	154.1	108.3
	138.9	111.5	149.9	147.4	118.5	-	135.1	104.2	154.7	131.1	154.7	104.2
	132.5	114.5/115.7	150.9	148.5	112.7	118.8/122.5	135.0/138.1	106.6	155.0	134.2	155.6	106.6
	133.6	113.7	151.9	146.5	116.2	-						
	133.6	113.5	153.8	147.2	117.5	-						
WT-32A	130.3/136.6	111.6/109.5	148.4	145.1	-	-	-	104.6/108.5	152.9	135.4	152.9	104.6/108.5
	136.4	114.6	149.4	146.1	113.8	-	-	103.8	154.7	134.4	154.7	103.8
	136.4	113.9	152.0	146.4	113.8	-	-	104.6/108.5	153.2	137.6	153.2	104.6/108.5
	136.3/135.4	110.7/116.8	151.3	148.7	116.5	-	-	104.6/108.5	153.7	132.2	154.0	104.6/108.5
	132.7/134.7	112.8/110.8	152.8	147.0	116.7/113.5	-	-	104.6/108.5	153.3	141.5	153.3	104.6/108.5
	134.7	-	-	-	-	119.8	-	-	153.6	144.1	153.6	-
	132.6	-	-	-	-	120.5	134.8	106.5	-	-	-	106.5
	-	-	153.6	144.1	-	-						
	-	-	153.6	144.1	-	-						
ref3-16A	135.7/132.1	113.2/111.5	147.7	143.5	-	-	136.4	103.3	153.2	134.0	153.2	103.3
	135.7/132.1	113.2/111.5	148.7	144.6	118.9	-	136.4/134.5	103.5/108.6	153.8	132.9	153.8	103.5/108.6
	135.7/132.1	113.2/111.5	148.5	145.8	118.5	-	137.0	102.7	152.6	136.0	152.6	102.7
	133.6	113.5	150.8	146.4	117.8	124.2	137.0	102.8	152.4	138.8	152.4	102.8
	136.6	110.4	150.4	147.7	115.7	-	-	-	151.2	140.8	151.2	-
	129.2	112.4	153.0	146.5	117.8	124.2	136.2	106.2	-	-	-	106.2
	129.2	112.4	152.7	148.2	115.3	-						
	129.2	112.4	152.3	149.6	116.9	-						
fah1-16A	136.2/138.1	109.6/112.9	148.8	146.1	-	-						
	136.8	113.8/114.8	149.7	146.3	-	-						
	129.8/136.2	113.6/116.7	150.1	147.6	114.0	119.5						
	133.1/136.6	112.8/114.8	152.1	146.8	115.5	-						
	133.1/138.1	112.8/110.4	153.3	148.8	118.5	119.9						
	133.1/138.1	112.8/110.4	153.3	141.5	-	-						
	-	-	-	150.6	116.7	120.3						
	131.5	-	-	-	-	123.8						
	131.0/133.5	-	-	-	-	120.0						
	133.0	-	-	-	-	118.0						
	134.3/136.5	-	-	-	-	122.6						

* Some G lignin C3 and C4 have chemical shift values overlapping with S3/5, and these sites are indicated as G'3/4 in the figures.

Supplementary Table 5. Integration areas for solid-state NMR spectral analysis. F_2 = direct ^{13}C dimension; F_1 = indirect ^{13}C dimension. S/G: deprotonated lignin aromatic carbons, i.e., S(1, 3-5) and G(1,3-4); Carbo: carbohydrate sites including i/s(1-6), Xn(1-5) and GalA(1-5); OMe: lignin methoxy carbons; AcMe: acetyl methyl carbons; CO: carbonyl carbons, including those from acetyl and C6 of GalA. The spectral regions (A1-A4 and B1-B8) are shown in Supplementary Fig. 5.

Spectra	Integral Name	Integral Region (F_2) (ppm)	Integral Region (F_1) (ppm)	^{13}C sites/ ^{13}C pairs	Integration Analysis	Analysis Description
1D CP 1D DP 1D cross-section of gated PDSD	A1	190.0 – 0.0	-	All ^{13}C	A3/A1	1D CP analysis, rigid lignin content in the whole cell
	A2	106.0 – 59.0	-	Carbohydrate ^{13}C i/s(1-6) Xn(1-5) GalA(1-5)		
	A3	156.0 – 109.0	-	Lignin ^{13}C* S(1, 3-5) G(1-6)	(A4/A1) in DP / (A4/A3) in CP	1D DP analysis, quantitative lignin content in the whole cell
	A4	156.0 – 140.0	-	S(3/5) G(3/4)	A2/A1	1D cross-section of 2D gated PDSD analysis, specific carbon site to carbohydrate transfer
2D Gated PDSD	B1	180.0 – 15.0	124.0 – 160.0	All ^{13}C propagated from S/G	(B3+B4+B5+B6+B7+B8)/(B1+B2)	(S/G+OMe) – (Carbo+CO+AcMe)
	B2	180.0 – 15.0	52.0 – 58.5	All ^{13}C propagated from OMe	(B3+B4)/(B1+B2)	(S/G+OMe) – Carbo
	B3	106.5 – 59.0	124.0 – 160.0	S/G – Carbohydrate	(B5+B6+B7+B8)/(B1+B2)	(S/G+OMe) – (CO+ AcMe)
	B4	106.5 – 59.0	52.0 – 58.5	OMe – Carbohydrate	B3/B1	S/G – Carbo
	B5	177.0 – 168.0	124.0 – 160.0	S/G – CO	(B5+B6)/B1	S/G – (CO+ AcMe)
	B6	24.0 – 17.0	124.0 – 160.0	S/G – AcMe	B5/B1	S/G – CO
	B7	177.0 – 168.0	52.0 – 58.5	OMe – CO	B6/B1	S/G – AcMe
	B8	24.0 – 17.0	52.0 – 58.5	OMe – AcMe	B4/B2	OMe - Carbo
					(B7+B8)/B2	OMe – (CO+ AcMe)
					B7/B2	OMe – CO
					B8/B2	OMe – AcMe
2D Gated DARR	A1	106.0 – 103.5	172.0 – 174.0	AcCO – $Xn^{2f}(1)$	A1/(A1+A2+A3)	acetyl groups in Xn^{2f}
	A2	103.5 – 101.5	172.0 – 174.0	AcCO – $Xn^{3f}(1)$	A2/(A1+A2+A3)	acetyl groups in Xn^{3f}
	A3	101.5 – 99.5	172.0 – 174.0	AcCO – GalA(1)	A3/(A1+A2+A3)	acetyl groups in GalA
2D refocused INADEQUATE	I1	156.0 – 150.0	283.0 – 295.0	S3/5	I1/(I1+I3)	S in the overlapping region
	I2	141.0 – 130.0	283.0 – 295.0	S4	I3/(I1+I3)	G in the overlapping region
	I3	156.0 – 150.0	295.0 – 307.0	G3/4	[(I1+I2)/2]/[(I1+I2)/2+(I1+I3)]	S content estimated in DQSQ
	I4	150.0 – 141.0	288.0 – 307.0	G3/4	(I1+I2)/[(I1+I2)/2+(I1+I3)]	G content estimated in DQSQ

*Aromatic residue sidechain and fatty acid chain carbon sites in the A3 region of 1D are at 136, 130 and 128.5 ppm and only show up in the 1D DP

Supplementary Table 6. Solution NMR experimental parameters. NUS = Non-Uniform Sampling; B_0 = magnetic field; NS = number of scans; d1 = recycle delay; SW = spectral width; t2/t1 = acquisition length for the direct/indirect dimension; TD2/TD1 = total points of FID for the direct/indirect dimension acquisition; Expt = Experiment Time.

Sample	Experiment	T (K)	B_0 (T)	NS	NUS amount	d_1 (s)	SW (ppm)	t_2/t_1 (ms)	TD2/TD1	Expt
WT-16A	1D DP (^{13}C)	298	11.7	2048	-	2.0	240	1087.9	65536	1h48m
	2D HSQC (^{1}H/^{13}C)	298	14.1	512	75%	0.7	13/220	131.1/3.8	2048/256	23h25m
fah1-16A	1D DP (^{13}C)	298	11.7	2048	-	2.0	240	1087.9	65536	1h48m
	2D HSQC (^{1}H/^{13}C)	298	14.1	512	75%	0.7	13/220	131.1/3.8	2048/256	23h25m
ref3-16A	1D DP (^{13}C)	298	11.7	2048	-	2.0	240	1087.9	65536	1h48m
	2D HSQC (^{1}H/^{13}C)	298	14.1	512	75%	0.7	13/220	131.1/3.8	2048/256	23h25m

Supplementary References

1. van Meerten, S.G.J., Franssen, W.M.J. & Kentgens, A.P.M. ssNake: A cross-platform open-source NMR data processing and fitting application. *J. Magn. Reson.* **301**, 56-66 (2019).